© 2018. Published by The Company of Biologists Ltd | Development (2018) 145, dev163105. doi:10.1242/dev.163105

RESEARCH ARTICLE

Lats1/2 inactivation reveals Hippo function in alveolar type I cell differentiation during lung transition to air breathing

Leah B. Nantie[1], Randee E. Young[1,2], Wyatt G. Paltzer[2], Yan Zhang[1,2], Randy L. Johnson[3], Jamie M. Verheyden[2] and Xin Sun[1,2,*]

ABSTRACT

Lung growth to its optimal size at birth is driven by reiterative airway branching followed by differentiation and expansion of alveolar cell types. How this elaborate growth is coordinated with the constraint of the chest is poorly understood. Here, we investigate the role of Hippo signaling, a cardinal pathway in organ size control, in mouse lung development. Unexpectedly, we found that epithelial loss of the Hippo kinase genes *Lats1* and *Lats2* (*Lats1/2*) leads to a striking reduction of lung size owing to an early arrest of branching morphogenesis. This growth defect is accompanied by abnormalities in epithelial cell polarity, cell division plane and extracellular matrix deposition, as well as precocious and increased expression of markers for type 1 alveolar epithelial cells (AEC1s), an indicator of terminal differentiation. Increased AEC1s were also observed in transgenic mice with overexpression of a constitutive nuclear form of downstream transcriptional effector YAP. Conversely, loss of *Yap* and *Taz* led to decreased AEC1s, demonstrating that the canonical Hippo signaling pathway is both sufficient and necessary to drive AEC1 fate. These findings together reveal unique roles of Hippo-LATS-YAP signaling in the developing mouse lung.

KEY WORDS: Lung, Development, Hippo, Branching, Alveolar, Polarity, Mouse

INTRODUCTION

The mechanical properties of the developing lung undergo dynamic changes *in utero*. Early on during pseudoglandular branching, proliferating epithelial cells jostle for space within the growing monolayer and push against surrounding mesenchymal cells and extracellular matrix (ECM) to extend the epithelial tips following a stereotypical program (Metzger et al., 2008; Lefevre et al., 2017). Later, during canalicular branching and sacculation, fluid pressure in both the epithelial lumen and plural space between the lung and the chest wall leads to an increase in mechanical pressure on all cell types in the lung. After birth, fluid is replaced with air, which, with each breath, exerts tidal pressure on lung cell types. How these dynamic mechanical properties impact cell proliferation, apical-basal polarity and cell fate choices during lung development remains poorly understood.

The Hippo signaling pathway is a conserved kinase cascade that senses the cellular environment, such as matrix stiffness, to regulate diverse cellular processes, including cell proliferation, movement, polarity and differentiation (Pan, 2010; Piccolo et al., 2014; Mo et al., 2014). There is emerging evidence that Hippo signaling controls the expression of genes responsible for ECM production, including *Ctgf*, *Cyr61* and *Lama5*, demonstrating a feedback mechanism (Zhao et al., 2008; Chang et al., 2015). Canonical Hippo pathway components include the upstream kinases MST1 and MST2 (STK3) that phosphorylate LATS1/2, which in turn phosphorylate YAP/TAZ, leading to their retention in the cytoplasm and subsequent degradation. When Hippo signaling is disrupted, the kinases are inactive, therefore unphosphorylated YAP/TAZ proceed to enter the nucleus and form a complex with transcriptional co-factors to influence target gene transcription. YAP/TAZ transcriptional targets often include positive regulators of cell proliferation and negative regulators of cell death. Thus, inactivation of Hippo signaling leads to enlarged organ size, a signature phenotype of the pathway (Pan, 2010; Mo et al., 2014).

Several recent studies investigated the roles of Hippo pathway in lung development and compensatory re-growth after pneumonectomy by inactivating either *Yap* or *Mst1/2* (Lin et al., 2015; Chung et al., 2013; Lange et al., 2015; Liu et al., 2016). The results have led to conflicting conclusions and left gaps in knowledge. For example, in the *Mst1/2* deletion mutants, one study showed that both type 1 (AEC1) and type 2 (AEC2) alveolar epithelial cells are decreased and YAP phosphorylation is not affected (Chung et al., 2013), whereas others show that AEC1 and AEC2 number are differentially affected and YAP phosphorylation is affected (Lange et al., 2015; Lin et al., 2015). There is not a major change in organ size in any of the *Mst1/2* mutants.

To clarify and substantiate how Hippo signaling affects the developing lung epithelium, we investigated the role of *Lats1/2*, which encode the most proximal kinases to YAP, by inactivating these genes in the lung epithelium. Early inactivation at the start of lung development led to a drastic decrease, rather than the expected increase of lung size. Although lung specification did occur, *Lats1/2* mutant lungs showed the most profound branching disruption observed in all Hippo pathway lung mutants examined to date. Accompanying the branching defect was a striking precocious expression of AEC1 markers. This promotion of terminal differentiation of the squamous AEC1 cell fate is recapitulated in constitutive nuclear YAP overexpression during sacculation. In contrast, there is a decrease in AEC1 markers in YAP/TAZ loss-of-function mutants. Our results suggest that proper Hippo signaling is crucial for proper control of AEC1 fate as the lung transitions to the extra-uterine environment.

RESULTS

Lats1/2 inactivation led to a minute lung with complete halt of secondary branching morphogenesis

We quantified transcript levels of *Lats1* and *Lats2* in embryonic day (E) 11.5, E15.5 and E18.5 control lungs and found that *Lats1* and

[1]Laboratory of Genetics, Department of Medical Genetics, University of Wisconsin-Madison, Madison, WI 53706, USA. [2]Department of Pediatrics, Department of Biological Sciences, University of California-San Diego, La Jolla, CA 92093, USA. [3]Department of Cancer Biology, University of Texas, MD Anderson Cancer Center, Houston, TX 77030, USA.

*Author for correspondence (xinsun@ucsd.edu)

X.S., 0000-0001-8387-4966

Received 6 January 2018; Accepted 3 October 2018

Development (2018) 145, dev163105. doi:10.1242/dev.163105

Lats2 mRNA levels remain relatively constant throughout development (Fig. S1). To determine whether *Lats1* and *Lats2* are required for lung development, we generated mice with loss of *Lats1* and *Lats2* in the developing lung epithelium, using Shh^{cre}, which drives robust Cre activity in the lung epithelium starting at lung specification (Shh^{cre};$Lats1^{del/fl}$;$Lats2^{del/fl}$; hereafter *Shhcre;Lats* mutants) (Harris et al., 2006). Although loss of LATS is known to result in grossly increased organ size in multiple contexts, among a number of gross morphological defects, *Shhcre;Lats* mutant lungs were greatly reduced in size at E18.5 (Fig. 1A, Fig. S2) (Dong et al., 2007; Camargo et al., 2007). This unexpected result, along with previous studies suggesting that Hippo signaling may not act through YAP in the developing lung, led us to investigate whether canonical Hippo signaling is disrupted in *Shhcre;Lats* mutants (Chan et al., 2013). At E11.5, phosphorylated YAP (p-YAP) was detected in the cytoplasm of epithelial and mesenchymal cells in control lungs (Fig. 1B), and was near absent specifically in the epithelial cells in *Shhcre;Lats* mutants (Fig. 1C). At E10.5 and E11.5 in control lungs, total YAP was detected throughout the nucleus and cytoplasm of epithelial and mesenchymal cells (Fig. 1D, Fig. S3A). In *Shhcre;Lats* lungs, although mesenchymal expression remains unchanged, YAP was present exclusively in the nucleus in epithelial cells (Fig. 1E, Fig. S3B). Additionally, whole-lung qRT-PCR analysis indicated that transcript levels of YAP target genes, such as *Ctgf* and *Amotl2*, were increased in *Shhcre;Lats* mutants, suggesting that YAP transcriptional activity is increased (Fig. S3C). These data suggest that in the developing lung epithelium, LATS is required for phosphorylation and cytoplasmic retention of YAP.

To address the cause of size reduction, we traced the phenotype to earlier stages. In E10.5 *Shhcre;Lats* mutants, NKX2-1 expression was unchanged, suggesting that the lung fate is properly specified (Fig. S3D,E). Primary budding occurred in the mutant; however, by E11.5 primary lung buds failed to undergo secondary branching morphogenesis (Fig. 1F-H). Additionally, the epithelium of *Shhcre;Lats* mutant lungs appeared multilayered, with disorganized cells extruding into the lumen (Fig. 1I-N). This complete halt of secondary branching morphogenesis is much more severe than that in Shh^{cre};*Mst1;Mst2* (hereafter *Shhcre;Mst*) mutants, in which growth defects were first detected during sacculation (Lin et al., 2015; Chung et al., 2013; Lange et al., 2015). Also different from the *Shhcre;Mst* mutants, cell proliferation was unchanged in the epithelium of *Shhcre;Lats* mutant lungs (Fig. S4A-C). In contrast, apoptotic cell death was increased, especially in the extruded luminal cells (Fig. S4D,E). These data indicate that loss of *Lats1/2* led to one of the strongest phenotypes yet observed among lung development mutants, and had a much more severe impact than loss of their upstream kinases, *Mst1/2*.

Lats1/2 are required for proper proximal/distal lung patterning

To determine whether the branching defect is also accompanied by a patterning defect, we stained E11.5 lungs with anti-SOX2 and anti-SOX9 antibodies as proximal and distal markers, respectively. In contrast to a robust expression of these markers in the control, in the *Shhcre;Lats* mutants, SOX2 was weakly detected in a proximal subset of epithelial cells that extruded apically into the lumen, whereas SOX9 was weakly detected in a distal subset of the epithelial cells that were positioned more basally in the abnormally multilayered epithelium (Fig. 2A,B). The reduction of staining for SOX9 protein was corroborated by whole-lung qRT-PCR of *Sox9*

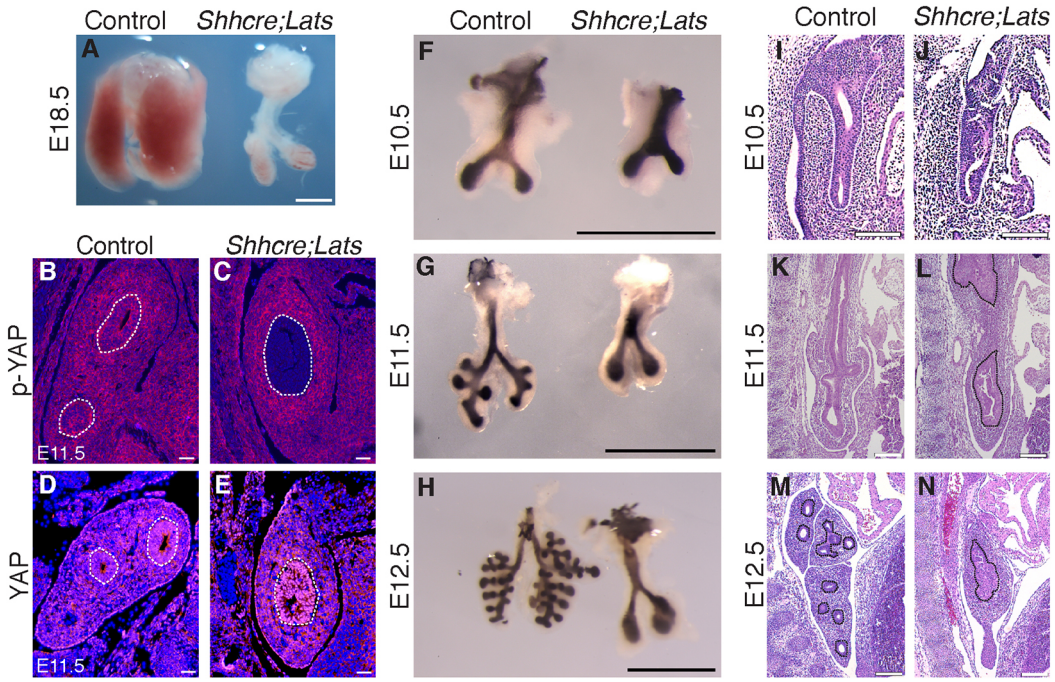

Fig. 1. *Shhcre;Lats* mutants displayed impaired branching morphogenesis. (A) Whole lungs of control and *Shhcre;Lats* mutant mice at E18.5. (B,C) Immunofluorescent detection of p-YAP (red) in control and *Shhcre;Lats* mutant lungs at E11.5, showing near absence of signal in the mutant epithelium. (D,E) Immunofluorescent detection of YAP (magenta) in control and *Shhcre;Lats* mutant lungs at E11.5, showing intense nuclear staining in the mutant epithelium. Blue, DAPI (B-E). (F-H) E-cadherin whole-mount immunohistochemistry outline of the epithelium in E10.5-E12.5 control and *Shhcre;Lats* mutant lungs showing the lack of branching in mutant lungs. (I-N) Hematoxylin and Eosin staining of sagittal sections of E10.5-E12.5 control and *Shhcre;Lats* mutant lungs, showing thickened epithelium at all stages. Dashed lines outline the epithelium. Scale bars: 50 µm (B-E,I-N); 1 mm (A,F-H).

Development (2018) 145, dev163105. doi:10.1242/dev.163105

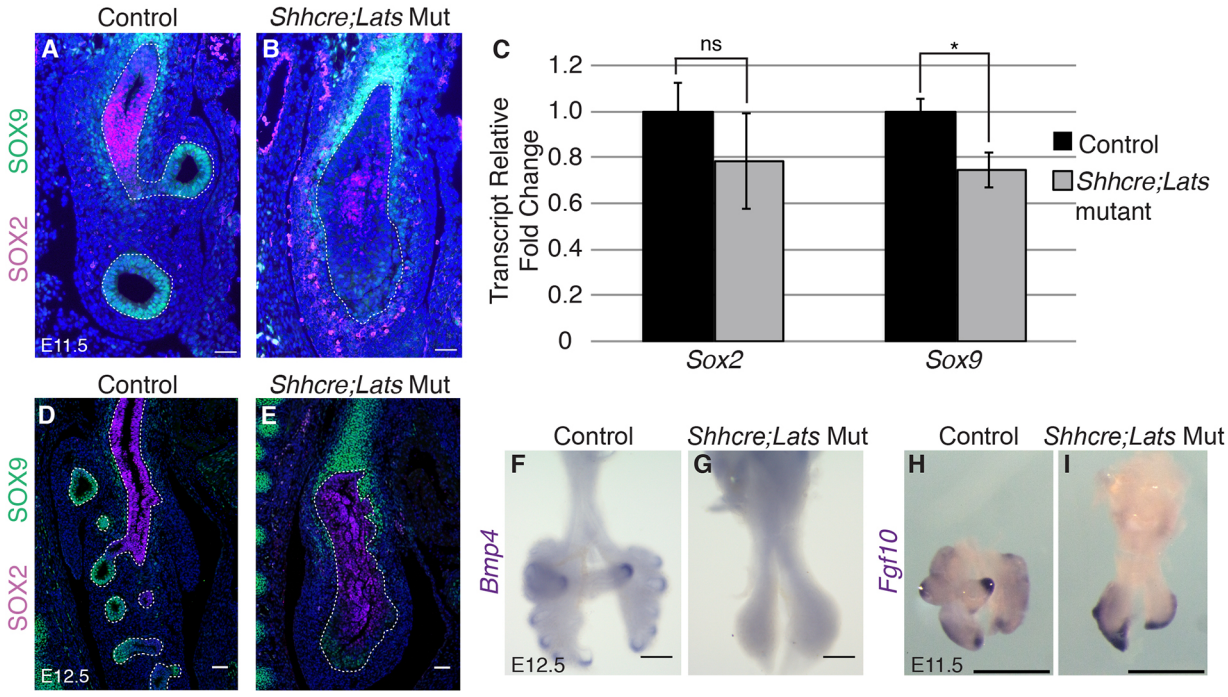

Fig. 2. *Shhcre;Lats* mutants showed defective proximal-distal patterning markers at E11.5. (A,B,D,E) Immunofluorescent detection of SOX2 (magenta) and SOX9 (green) in control and *Shhcre;Lats* mutant lungs at E11.5 (A,B) and E12.5 (D,E) showing disrupted expression of these proximal-distal markers compared with control. Blue, DAPI. (C) Quantification of relative mRNA levels of *Sox2* and *Sox9* in *Shhcre;Lats* mutant lungs at E11.5. Data are presented as mean±s.e.m. **P*<0.05 (Student's *t*-test). ns, not significant. (F-I) Whole-mount RNA *in situ* hybridization showing reduction of *Bmp4* expression in the distal epithelium, and expansion of *Fgf10* expression in the mesenchyme of *Shhcre;Lats* mutant lungs compared with controls. Dotted lines outline the epithelium. Scale bars: 50 µm (A, B,D-G); 100 µm (H,I).

transcripts (Fig. 2C), even though the expression change in the epithelium may be dampened by persisting expression in the mesenchyme. The level of *Sox2* transcripts also appeared to be decreased although this was not statistically significant (Fig. 2C). Similarly disrupted SOX2 and SOX9 expression was also observed at E12.5, although SOX2 expression appeared to be higher than at E11.5 (Fig. 2D,E). These results indicate that both proximal and distal markers are present, but compromised, in the *Shhcre;Lats* mutants.

Additionally, we investigated the expression of *Bmp4* and *Fgf10*, essential factors for branching morphogenesis. *Bmp4* was expressed in the distal epithelium of control lungs at E12.5 (Fig. 2F) and was absent from the epithelium of *Shhcre;Lats* mutants (Fig. 2G). Conversely, *Fgf10* was expressed in the distal mesenchyme of control lungs at E11.5 (Fig. 2H) and was expanded in the mesenchyme of *Shhcre;Lats* mutants (Fig. 2I). These data suggest that the expression of key branching factors *Bmp4* and *Fgf10* is disrupted downstream of LATS.

Lats1/2 are required for proper apical-basal polarity in the developing lung

To determine the cellular mechanism underlying branching and patterning defects, we examined several markers of basic cellular properties. E-cadherin (CDH1), the major component of adherens junctions, is required for proper branching in the submandibular gland and mammary gland (Walker et al., 2008; Boussadia et al., 2002). In the control lung, as expected, E-cadherin staining was more intense in the apical-lateral surfaces than the basal surface. In *Shhcre;Lats* mutant lungs, there was a loss of the apical bias and an increase of staining intensity in the basal epithelium (Fig. 3A-D). This increase in staining was corroborated by qRT-PCR results showing elevated transcripts (Fig. 3E).

The altered subcellular localization of E-cadherin suggests that apical-basal polarity may be disrupted in *Shhcre;Lats* mutants. Disruptions in apical-basal polarity also led to defective branching morphogenesis in multiple organs, including the lung (Yates et al., 2013; Chen et al., 2010). In control lungs at E11.5, atypical protein kinase C (aPKC) was detected with a consistent intensity bias in the apical domain of epithelial cells. In contrast, aPKC was detected throughout the entire epithelium in *Shhcre;Lats* mutants (Fig. 3F,G). Conversely, scribble (SCRIB) was detected with a consistent bias in the basolateral domain of control epithelial cells, and was detected in a disorganized pattern in the epithelium of *Shhcre;Lats* mutants (Fig. 3H,I), such that some cells had decreased SCRIB expression, whereas others had cortical SCRIB expression. Apical-basal polarity is often linked to deposition of basement membrane proteins. In the control, laminin α5 was restricted to the basement membrane underlying the epithelium at E11.5. However, in the mutant, it was extended apically through the lateral space between cells (Fig. 3J,K).

The gross phenotype of *Shhcre;Lats* mutants resembles that of the *Shhcre;Itgb1* mutants, in which the integrin β1 (*Itgb1*) gene is inactivated in the developing lung epithelium (Chen and Krasnow, 2012). We found that integrin β1 (ITGB1) protein is expressed in a similar pattern in the control and in *Shhcre;Lats* mutants (Fig. 3L,M). Conversely, YAP was expressed in a similar pattern to control in the *Shhcre;Itgb1* mutant (Fig. S5). These data suggest that ITGB1 and LATS function in parallel to maintain the single-layer epithelium in the developing lung.

Taken together, these findings demonstrate that *Shhcre;Lats* mutants have altered localization of specific adhesion molecules, apical-basal polarity determinants and ECM/basement membrane components. These disrupted elements are likely to be contributing factors to the halt of branching in these mutants.

Development (2018) 145, dev163105. doi:10.1242/dev.163105

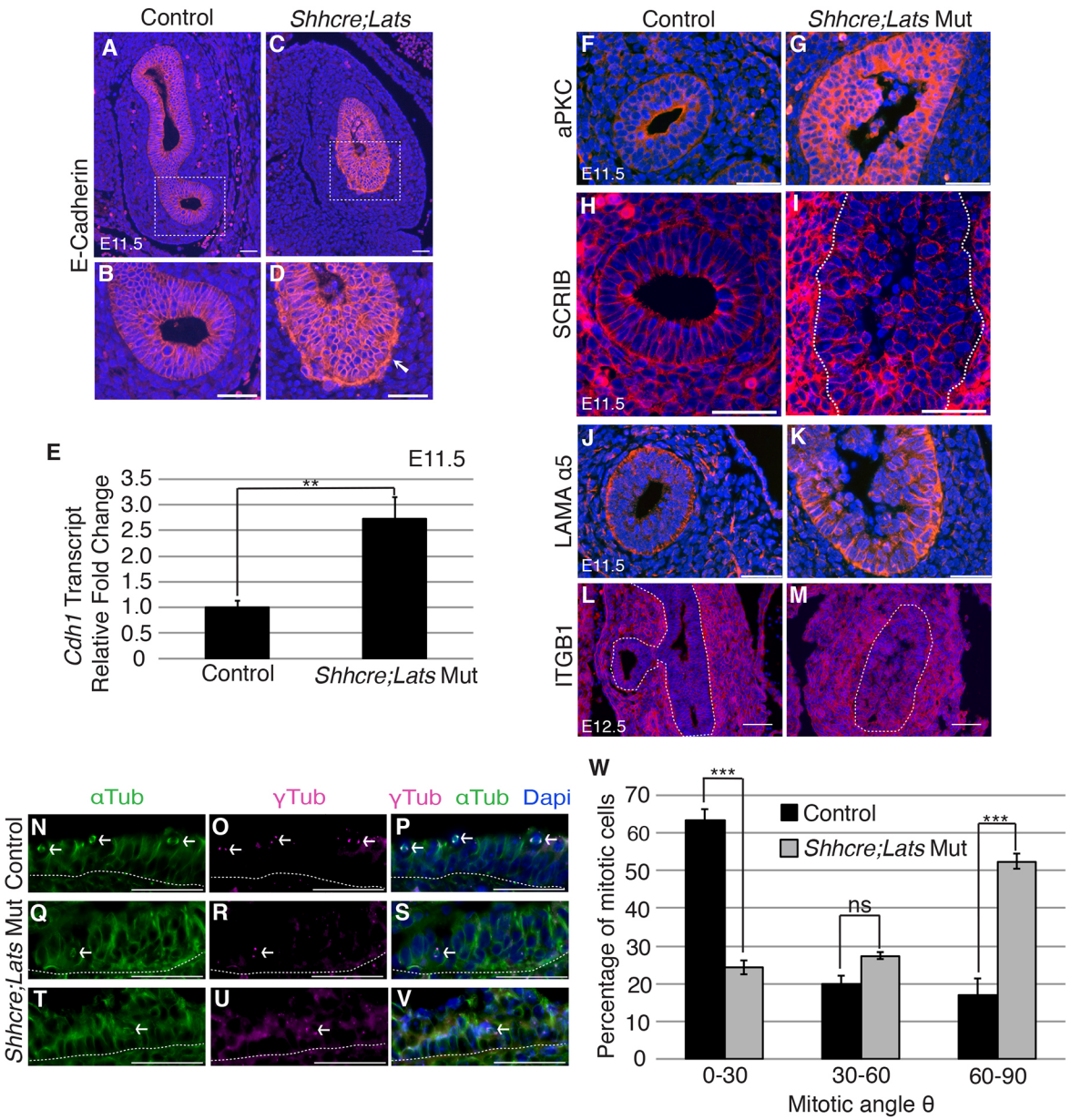

Fig. 3. *Shhcre;Lats* mutants showed impaired apical basal polarity and mitotic spindle angle. (A-D) Immunofluorescent detection of E-cadherin (red, arrow) in control and *Shhcre;Lats* mutant lungs at E11.5. Lower panels show magnifications of the boxed areas in the upper panels. E-cadherin signal is increased and less apically biased in the mutant. Arrow indicates the basal epithelium. (E) qRT-PCR quantification of relative levels of *Cdh1* mRNA in control and *Shhcre;Lats* mutant lungs at E11.5. (F,G) Immunofluorescent detection of aPKC (red) in control and *Shhcre;Lats* mutant lungs at E11.5, showing loss of apical bias and expansion of signal in the mutant epithelium. (H,I) Immunofluorescent detection of SCRIB (red) in control and *Shhcre;Lats* mutant lungs at E11.5, showing loss of lateral/basal bias of signal in the mutant epithelium. Dotted line outlines epithelium. (J,K) Immunofluorescent detection of LAMAα5 (red) in control and *Shhcre;Lats* mutant lungs at E11.5, showing loss of basal restriction of signal in the mutant. (L,M) Immunofluorescent detection of ITGB1 (red) at E12.5, showing similar expression in control and *Shhcre;Lats* mutant lungs. (N-V) Immunofluorescent detection of centrosomes (γTub, magenta) and microtubules (αTub, green) in control and *Shhcre;Lats* mutant lungs at E11.5. Arrows indicate mitotic spindles. (W) Quantification of mitotic spindle angle θ, the mitotic spindle angle relative to the basement membrane in control and *Shhcre;Lats* mutant lungs at E11.5. Data are presented as mean±s.e.m. ***P*<0.005, ****P*<0.001 (Student's *t*-test). ns, not significant. Scale bars: 50 µm (A-D,F-K,N-V); 100 µm (L,M). Dotted lines outline epithelium. Blue, DAPI.

Lats1/2 are required for proper mitotic spindle angle during epithelial proliferation

The alterations in apical-basal polarity may lead to a greater propensity of the mutant epithelial cells to divide at an angle perpendicular to the basement membrane, resulting in the multilayered epithelium in *Shhcre;Lats* mutants. To test this possibility, we outlined the dividing spindle with γ-tubulin and α-tubulin antibodies in E11.5 lungs. Whereas the majority of control epithelial cells divided parallel to the basement membrane (θ<30) to extend the epithelium lengthwise, the majority of *Shhcre;Lats* mutant epithelial cells divided perpendicular to the basement membrane (60<θ<90). Additionally, whereas the dividing spindles were mostly found near the apical surface in control lungs, they were found more randomly throughout the epithelium in the mutant lungs (Fig. 3N-W). This change in cell division could contribute to the accumulation of extra cell layers as well as failed tube elongation, which is key to branching morphogenesis.

Development (2018) 145, dev163105. doi:10.1242/dev.163105

Lats1/2 are required to restrict AEC1 cell differentiation

Because inactivation of *Shhcre;Lats* led to early arrest of branching morphogenesis, we investigated whether this also prevented all epithelial cell differentiation. At E18.5, when control lungs expressed markers of differentiated club cells (SCGB1A1), ciliated cells (FOXJ1), AEC2s (pro-SPC) and AEC1s (HOPX and PDPN), only AEC1 markers were detected in the *Lats1/2* mutant lungs (Fig. 4A-H). In the control, basal markers such as P63 (TRP63) and KRT5 were primarily restricted to the trachea, with little signal in the lung (Fig. 4I-K). In the mutant lung, however, we detected a small number of cells with a low level of P63 expression (Fig. 4L-N). There was very little overlap of P63 and HOPX expression (Fig. 4O-T). Of the few cells that were double positive for P63 and HOPX, it appeared that there was reduced HOPX expression compared with neighboring P63-HOPX^{+} cells (Fig. 4R-T, arrows). These findings indicate that loss of *Lats* leads to ectopic induction of both AEC1s and basal cells, the two epithelial cell types that show squamous morphology in the lung. It is notable that the ectopic AEC1s showed a more intense staining of the AEC1 marker HOPX in the mutant than in normal AEC1s in the

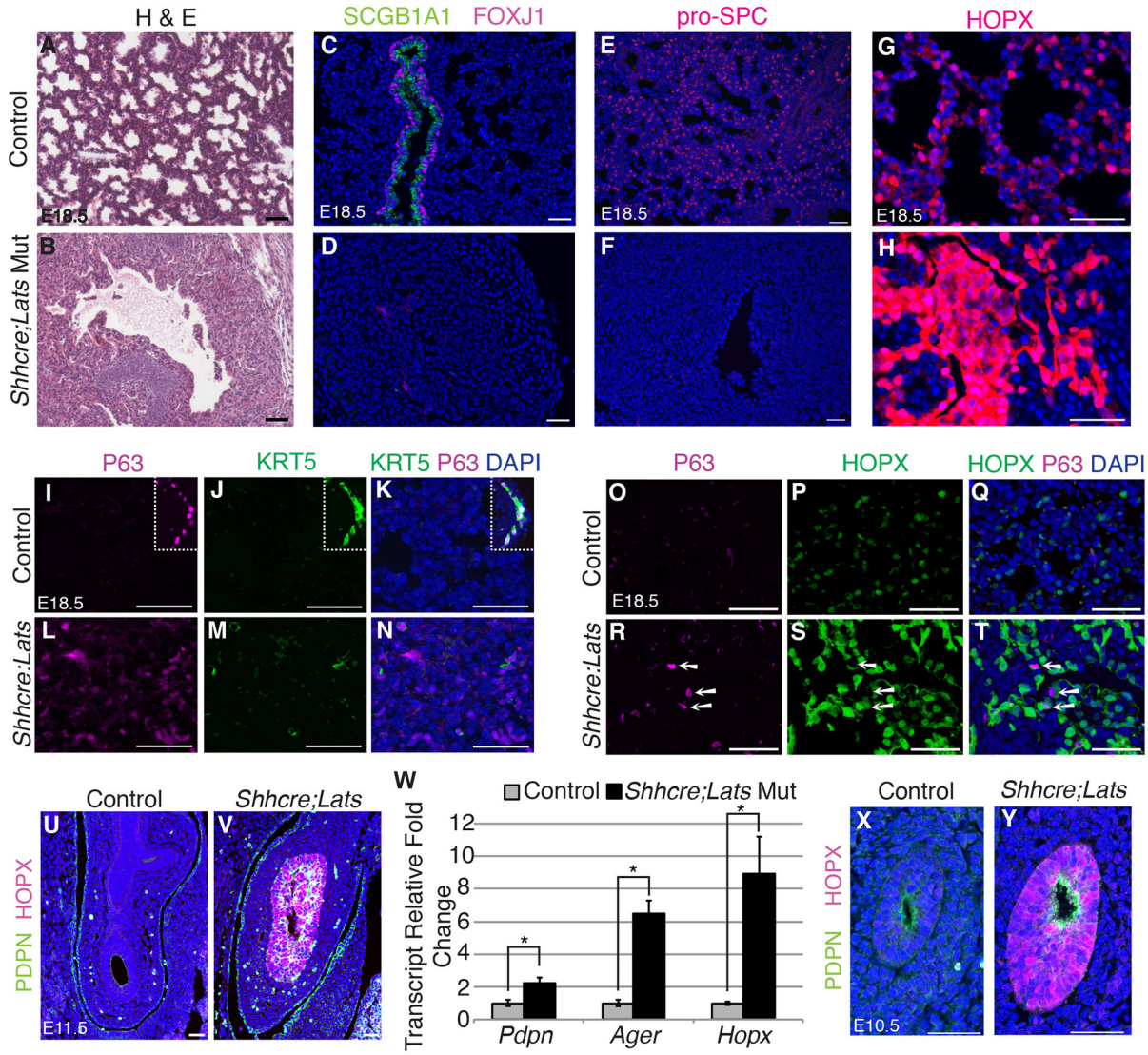

Fig. 4. *Shhcre;Lats* mutants showed increased expression of AEC1 markers. (A,B) Hematoxylin and Eosin staining of control and *Shhcre;Lats* mutant lungs at E18.5. The mutant image is centered on the left lobe, as are mutant images in the rest of the figure. (C,D) Immunofluorescent detection of SCGB1A1 (green) and FOXJ1 (red) in control and *Shhcre;Lats* mutant lungs at E18.5, showing loss of signal in the mutant. (E,F) Immunofluorescent detection of pro-SPC (red) in control and *Shhcre;Lats* mutant lungs at E18.5, showing loss of signal in the mutant. (G,H) Immunofluorescent detection of HOPX (red) in control and *Shhcre;Lats* mutant lungs at E18.5 at the same exposure time, showing drastically increased HOPX signal in the mutant. (I-N) Immunofluorescent detection of P63 (magenta) and KRT5 (green) in control and *Shhcre;Lats* mutant lungs at E18.5. Insets in I-K show P63 and KRT5 expression in the control trachea. When imaged and adjusted using the same parameters, the ectopic P63 and KRT5 signals in the mutant lung appear less intense compared with the trachea signal in the control. (O-T) Immunofluorescent detection of P63 (magenta) and HOPX (green) in control and *Shhcre;Lats* mutant lungs at E18.5. Arrows indicate P63^{+}HOPX^{+} cells, with low HOPX signal compared with surrounding P63^{-}HOPX^{+} cells. (U,V) Immunofluorescent detection of PDPN (green) and HOPX (magenta) in control and *Shhcre;Lats* mutant lungs at E11.5, showing increased signals of both in the mutant epithelium. (W) qRT-PCR quantification of relative mRNA levels of AEC1 markers *Pdpn*, *Ager* and *Hopx* in control and *Shhcre;Lats* mutant lungs at E11.5. Data are presented as mean±s.e.m. **P*<0.05 (Student's *t*-test). (X,Y) Immunofluorescent detection of PDPN (green) and HOPX (magenta) in control and *Shhcre;Lats* mutant lungs at E10.5, showing precocious expression of HOPX. Blue, DAPI. Scale bars: 50 µm.

Development (2018) 145, dev163105. doi:10.1242/dev.163105

control (Fig. 4P,Q,S,T), whereas the ectopic basal cells showed a less intense staining of basal markers in the mutant than in normal basal cells in the control (Fig. 4I-N).

In a normal lung, AEC1s are made in the distal alveolar region, whereas basal cells are made in the trachea, proximal to the lung. In the *Shhcre;Lats* mutant lung, the bias towards making ectopic AEC1s and fewer ectopic basal cells may be due to pre-existing distal patterning. To address this possibility, we assayed for the presence of these markers in the trachea where there is normally robust basal cell marker expression and little AEC1 marker expression. The trachea region of the *Shhcre;Lats* mutant had disrupted architecture with a large number of protruding cells filling the lumen (Fig. S6A-D). Many of the ectopic cells in *Shhcre;Lats* mutants expressed nuclear YAP, most of which also expressed HOPX. Similar to the lung, very few of the ectopic AEC1 cells expressed P63 (Fig. S6N-P). Although the trachea architecture was severely disrupted in *Shhcre;Lats* mutants, very little cell death was observed at E18.5 (Fig. S6Q,R). Together, the results from the trachea and lung suggest that when *Lats1/2* are lost, epithelial cells have the propensity to differentiate into either AEC1s or basal cells, with a preference towards AEC1s.

We traced the ectopic AEC1 phenotype to earlier stages. To our surprise, antibody staining revealed a striking premature expression of AEC1 markers HOPX and PDPN in mutant lungs at E11.5 (Fig. 4U,V). The increase was confirmed by qRT-PCR of multiple AEC1 markers (Fig. 4W) and was observed as early as E10.5, making it one of the earliest phenotypes observed in this mutant (Fig. 4X,Y).

Nuclear YAP is sufficient to induce expression of AEC1 markers

As there is a significant increase of nuclear YAP in the *Shhcre;Lats* mutant epithelium, we investigated whether this is sufficient to induce AEC1 fate. We generated mice with inducible expression of activated YAP in the lung epithelial cells, by breeding *tetO-YAP^{S127A}* to *Sftpc-rtTA* mice (hereafter *Sftpc-rtTA;tetO-YAP^{S127A}* mutants). In the alveolar region, when induced with doxycycline beginning at E15.5, a stage during which bipotent AEC1/AEC2 progenitors are first described (Desai et al., 2014), *Sftpc-rtTA;tetO-YAP^{S127A}* mutants exhibited increased AEC1s and decreased AEC2s compared with controls (Fig. 5A-N). Furthermore, 92.17% (±4.32%) of the cells with strong expression of nuclear YAP in *Sftpc-rtTA;tetO-YAP^{S127A}* mutants expressed the AEC1 marker HOPX, whereas only 2.05% (±0.71%) expressed the AEC2 marker pro-SPC (Fig. 5O). This induction of AEC1 cells was not restricted to the alveolar region. In the airway, cells in the *Sftpc-rtTA;tetO-YAP^{S127A}* mutant airway that strongly expressed nuclear YAP also expressed HOPX (Fig. S7), suggesting that the airway epithelium may retain some ability to differentiate into alveolar epithelial cell types at late stages of embryonic lung development. It is important to note that mutant cells with increased nuclear YAP expression did not proliferate at a higher frequency than control cells (control: 1.68±0.35%, n=3; *Sftpc-rtTA;tetO-YAP^{S127A}* mutant: 1.24%±0.23%, n=4) (Fig. S8), suggesting that the increase in AEC1s is not due to increased proliferation.

YAP and TAZ are necessary for AEC1 differentiation

The finding that nuclear Yap can induce AEC1 formation is consistent with the emergence of nuclear YAP in AEC1 cells as development proceeds into the adult (Fig. S9) (Liu et al., 2016). To determine whether *Yap/Taz* are also necessary for AEC1 differentiation, we generated mice with inducible loss of *Yap* and *Taz* in lung epithelial cells, by generating *Sftpc-rtTA;tetO-cre; Yap$^{fl/fl}$;Taz$^{fl/fl}$* mice (hereafter *Sftpc-rtTA;tetO-cre;Yap;Taz* mutants). When induced at E16.5, there was a decreased number of HOPX^{+} AEC1s in *Sftpc-rtTA;tetO-cre;Yap;Taz* mutants (Fig. 6A-C). The few cells that were able to differentiate into AEC1s in *Sftpc-rtTA;tetO-cre;Yap;Taz* mutants retained YAP nuclear expression, suggesting that they have escaped recombination (Fig. S10). The percentage of AEC2 cells out of total cells was not altered (Fig. 6D-F). *Sftpc-rtTA;tetO-cre; Yap$^{fl/fl}$;Taz$^{fl/+}$* lungs showed an intermediate phenotype, with fewer AEC1s than control mice, but more than *Sftpc-rtTA;tetO-cre;Yap;Taz* mutants, suggesting that YAP and TAZ act redundantly to promote full AEC1 differentiation (Fig. S10G-L).

DISCUSSION

Hippo signaling is most recognized for its role in regulating organ size. Specifically, disruption of the Hippo pathway kinase genes *Lats1/2* or *Mst1/2*, or their homologs *hippo* and *warts* in *Drosophila*, resulted in increased proliferation and decreased cell death, leading to larger organs (Pan, 2010). In the present study, we found that despite nuclear YAP localization in the epithelium, *Shhcre;Lats* mutants had smaller lungs, with a clear halt of development after primary branch formation, one of the more severe lung developmental phenotypes. Likely contributors to this defect are the disrupted localization of apical-basal polarity determinants, cell adhesion molecules and ECM components, and misorientation of the spindles of dividing cells. Instead of a single-cell layer epithelium, which is crucial for effective extension and growth of the branches, *Shhcre;Lats* mutants showed a multilayered epithelium with cells protruding into the lumen. Gross phenotypes similar to that of our *Lats1/2* mutant lungs were described in the kidneys and salivary glands of transgenics with overexpression of nuclear YAP or mutants with deletion of *Lats1/2* (Reginensi et al., 2016; Szymaniak et al., 2017). These findings suggest that in branching organs such as the lung, kidney and salivary gland, a primary role of Hippo signaling is to maintain an organized epithelium, which is cardinal for organ size.

The finding that determinants of adhesion and apical-basal polarity were altered in the *Shhcre;Lats* mutants revealed a feedback mechanism between these determinants and Hippo signaling. Many of these factors that we identified as being altered are also known to be upstream of Hippo signaling, including E-cadherin, which regulates YAP in human breast cancer cells (Kim et al., 2011), and aPKC, which regulates Yki (YAP equivalent in *Drosophila*) in the eye epithelium (Grzeschik et al., 2010). Similarly, Crb3, an apical-basal polarity determinant, regulates LATS phosphorylation and YAP localization in the developing lung epithelium (Szymaniak et al., 2015). This feedback control allows cells to not only respond to, but also modify, their microenvironment, ensuring coordinated morphogenesis and tissue growth.

This investigation, centered on *Lats1/2* mutants, builds on existing studies that have investigated the role of other Hippo pathway members in the developing lung, specifically *Mst1/2* and *Yap* (Lin et al., 2015; Szymaniak et al., 2015; Volckaert et al., 2017; Mahoney et al., 2014; Chung et al., 2013; Lange et al., 2015; Lin et al., 2017). As MST1/2 phosphorylate and activate LATS1/2, one would predict similar phenotypes from *Mst1/2* and *Lats1/2* epithelial mutants. However, whereas *Shhcre;Lats* mutants show a halt of branching at E10.5, *Shhcre;Mst* mutants have minimal branching defects (Lin et al., 2015; Lange et al., 2015). Indeed, LATS level and phosphorylation was not detectably decreased in *Mst* mutants (Lin et al., 2015). Furthermore, although E-cadherin and epithelial polarity

Development (2018) 145, dev163105. doi:10.1242/dev.163105

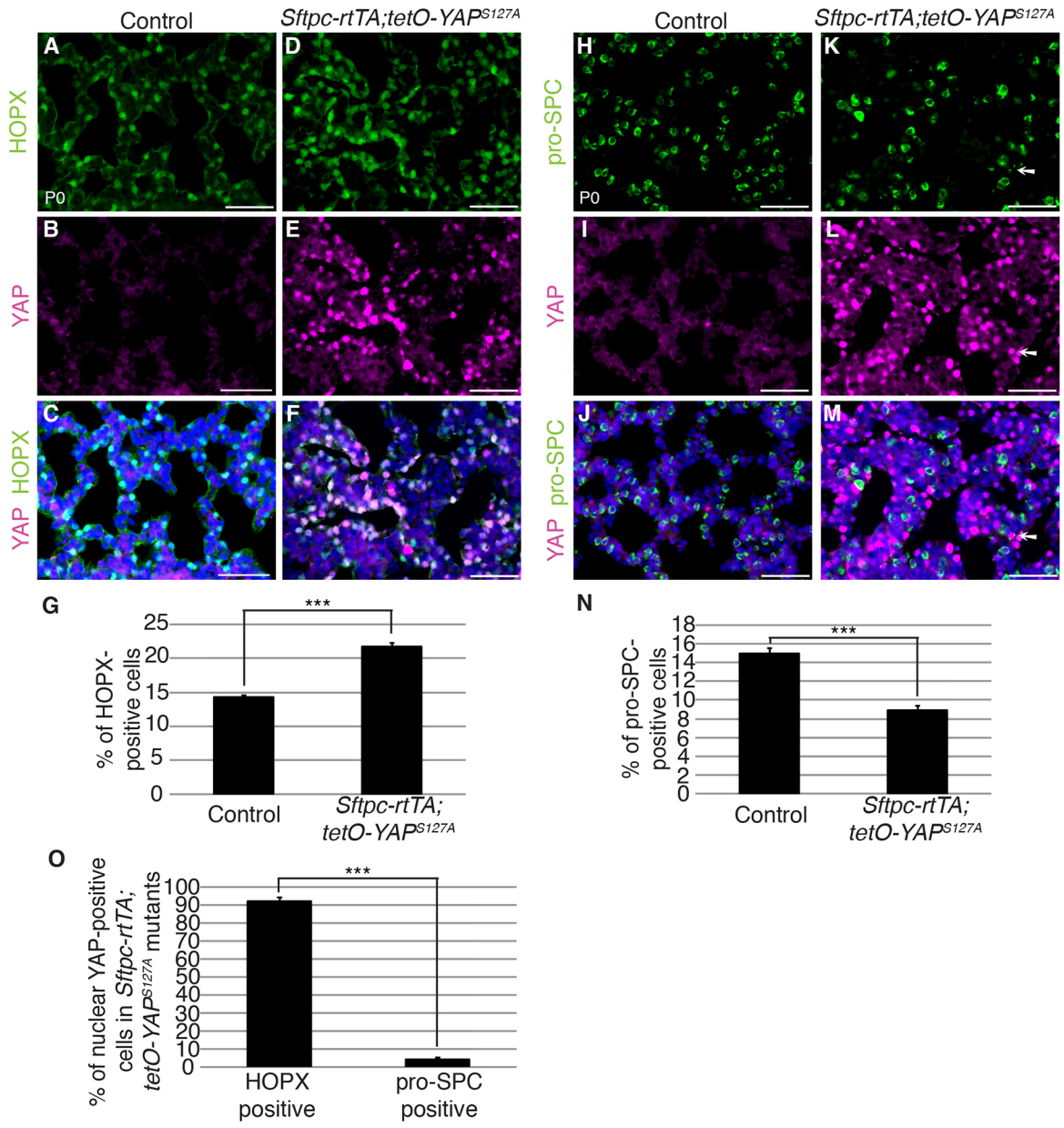

Fig. 5. *Sftpc-rtTA;tetO-YAP*^{S127A} mutants showed increased AEC1s and decreased AEC2s. (A-F) Immunofluorescent detection of HOPX (green) and YAP (magenta) in control and *Sftpc-rtTA;tetO-YAP*^{S127A} transgenic lungs at P0, showing that the majority of YAP^{+} cells are also HOPX^{+}. All images were taken at the same exposure. Nuclear YAP signal is more intense in the transgenic than in the control. (G) Quantification of the percentage of HOPX^{+} cells out of total cells in control and *Sftpc-rtTA;tetO-YAP*^{S127A} transgenic lungs at P0. (H-M) Immunofluorescent detection of YAP (magenta) and pro-SPC (green) in control and *Sftpc-rtTA;tetO-YAP*^{S127A} mutant lungs at P0, showing that very few (arrows) YAP^{+} cells remain SPC^{+}. Arrows indicate a double-labeled cell. (N) Quantification of the percentage of pro-SPC^{+} cells out of total cells in control and *Sftpc-rtTA;tetO-YAP*^{S127A} mutant lungs at P0. (O) Quantification of the percentage of cells with strong nuclear YAP and either HOPX or pro-SPC in *Sftpc-rtTA;tetO-YAP*^{S127A} mutant lungs at P0. Data are presented as mean±s.e.m. ***P<0.001 (Student's *t*-test). Blue, DAPI. Scale bars: 50 µm.

was minimally perturbed in *Mst* mutants during development, all three *Mst1/2* mutant studies showed increased epithelial proliferation (Lin et al., 2015; Chung et al., 2013; Lange et al., 2015), which was not observed in epithelial *Lats1/2* mutants. These findings suggest that it is not a linear path from MST1/2 to LATS1/2: LATS1/2 are likely regulated by factors other than MST1/2, and MST1/2 likely control factors in addition to LATS1/2.

Epithelial *Yap* mutants also exhibited branching defects. However, the epithelium remained largely a monolayer, different from that observed in the *Shhcre;Lats* mutants. It was suggested that the branching defect in the *Shhcre;Yap* mutant is due to inability of epithelial cells at the proximal-distal transition zone to respond to TGFβ signaling (Mahoney et al., 2014). However, another study of *Yap* mutants suggests that YAP controls lung branching by regulating proliferation and mechanical force production instead of proximal-distal patterning (Lin et al., 2017). In *Shhcre;Lats* mutants, we found that both SOX2 and SOX9 are decreased. The decrease is likely secondary to the earlier loss of apical-basal polarity and monolayer epithelial integrity. Although findings from *Shhcre;Lats* mutants do not resolve the debate on YAP function in branching, they suggest that MST/LATS/YAP and their co-factors control a complex network of targets.

Development (2018) 145, dev163105. doi:10.1242/dev.163105

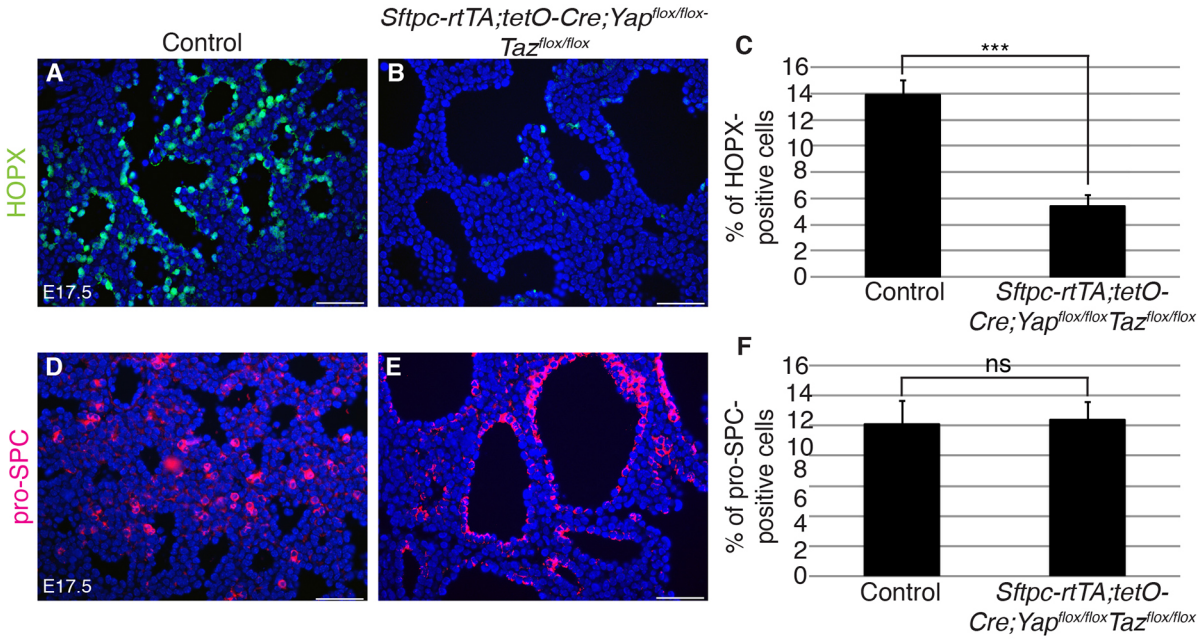

Fig. 6. *Sftpc-rtTA;tetO-cre;Yap*$^{flox/flox}$*;Taz*$^{flox/flox}$ mutants show decreased AEC1s. (A,B) Immunofluorescent detection of HOPX (green) in control and *Sftpc-rtTA;tetO-cre;Yap*$^{flox/flox}$*;Taz*$^{flox/flox}$ mutant lungs at E17.5 showing a drastic reduction of HOPX$^+$ cells. (C) Quantification of the percentage of HOPX$^+$ cells in control and *Sftpc-rtTA;tetO-cre;Yap*$^{flox/flox}$*;Taz*$^{flox/flox}$ mutant lungs out of total cell number at E17.5. (D,E) Immunofluorescent detection of pro-SPC (red) in control and *Sftpc-rtTA;tetO-cre;Yap*$^{flox/flox}$*;Taz*$^{flox/flox}$ mutant lungs at E17.5, showing presence of SPC$^+$ cells in the mutant. (F) Quantification of the percentage of pro-SPC$^+$ cells in control and *Sftpc-rtTA;tetO-cre;Yap*$^{flox/flox}$*;Taz*$^{flox/flox}$ mutant lungs out of total cell number at E17.5. Data are presented as mean±s.e.m. ***P<0.001 (Student's t-test). ns, not significant. Blue, DAPI. Scale bars: 50 µm.

Multiple lines of evidence support that inactivation of LATS1/2 or MST1/2, leading to accumulation of nuclear YAP, promotes progenitor cell state and inhibits differentiation (Zhao et al., 2014; Lin et al., 2015; Szymaniak et al., 2015; Chung et al., 2013; Lange et al., 2015; Volckaert et al., 2017). Consistent with this, there are increased basal cells, a progenitor cell type, in the trachea and lung of *Shhcre;Lats* mutants. In contrast, the strikingly precocious and increased expression of markers of AEC1, a lung epithelial cell type at the end of the chain of differentiation, offers an exception to the rule, and led us to reconsider the function of Hippo signaling in controlling cellular response to microenvironment.

Multiple studies have shown that YAP enters the nucleus in response to cell spreading (Lange et al., 2015; Aragona et al., 2013; Halder et al., 2012; Liu et al., 2016). In a pneumonectomy model of compensatory growth following re-section of a lung lobe, a CDC42-based mechanism responds to cell spreading in the alveolar region and sends YAP into the nucleus (Liu et al., 2016). In the airway, epithelial cells that spread out in response to injury recruit integrin-linked kinase, which destabilizes merlin (NF2) and inactivates MST/LATS, leading to increased nuclear YAP (Volckaert et al., 2017). In addition, there is also evidence that cellular flattening leads to loss of apical determinants such as Crb3, downregulation of LATS level and LATS phosphorylation, resulting in reduced YAP phosphorylation and increased accumulation of nuclear YAP (Szymaniak et al., 2015).

Our data from both the *Lats1/2* mutant as well as the *Sftpc-rtTA;tetO-YAP*^{S127A} mutant indicate that nuclear YAP could lead to either increased AEC1s or basal cells, the two 'flat' epithelial cell types in the lung. These cells can be specified despite reduced proximal-distal patterning markers. In addition, the AEC1s and basal cells are intermixed in the mutant lung and trachea regions, suggesting that the ability of nuclear YAP to induce these cells is independent of prior proximal-distal patterning. Further evidence suggests that these regulations may be direct. Genome-wide ChIP-Seq in cell lines and embryonic stem cells identified that YAP/TEAD bind enhancer regions of AEC1-specific genes, including *Pdpn* and *Ager* (Zhao et al., 2008; Zanconato et al., 2015). A co-immunoprecipitation experiment in basal cells showed that YAP and P63 directly interact, and ChIP-PCR experiments demonstrated that YAP can pull down regulatory regions of the same genes that P63 regulates in basal cells (Zhao et al., 2014). Interestingly, in the *Shhcre;Lats* mutant, although there is premature AEC1 differentiation, these cells are not squamous as are normal AEC1s. This is consistent with the notion that flat-cell fate can be separated from flat-cell morphogenesis. In the context of the lung, the fact that AEC1s are a terminally differentiated cell type whereas basal cells are progenitors indicates that the function of the Hippo pathway is not along the progenitor/differentiated cell divide. Rather, the Hippo pathway responds to upstream stretch and puts in motion the downstream differentiation program of epithelial cells with squamous morphology, the types of cells that are most sensitive to mechanical forces from the environment.

A previous study showed that in the adult lung following pneumonectomy, *Yap* is required in AEC2 cells for proliferation and differentiation into AEC1s (Liu et al., 2016). During development, our findings from *Yap* and *Taz* loss-of-function mutants suggest that *Yap* and *Taz* are required for AEC1 cell fate, but not AEC2 fate or number. This difference likely reflects the distinct requirements for these factors in development versus in adult injury repair.

Perinatally, as the lung transitions from being fluid-filled before birth to air-filled after birth, there is a drastic change of mechanical force in a short period of time. In coordination with the mechanical change, thinning of the distal epithelium from columnar to squamous AEC1 morphology is a crucial step for lung transition to the extra-uterine environment (Li et al., 2018). Large AEC1s tile to form the alveolar epithelial barrier. Their flatness allows close

Development (2018) 145, dev163105. doi:10.1242/dev.163105

engagement with the capillary network to enable efficient gas exchange. Findings in this study and from others demonstrate that LATS/YAP axis of Hippo signaling is essential for lung function at the moment of first breath.

MATERIALS AND METHODS

Mice

Lats1^{flox}, *Lats2*^{flox}, *Yap*^{flox}; *Taz*^{flox}; *tetO-YAP*^{S127A}; *Shh*^{cre}; *Sftpc-rtTA* and *tetO-cre* alleles and transgenic lines have been described before (Heallen et al., 2011; Xin et al., 2013; Xin et al., 2011; Camargo et al., 2007; Harfe et al., 2004; Perl et al., 2002a; Perl et al., 2002b). *Lats1*$^{flox/flox}$;*Lats2*$^{flox/flox}$ mice were bred to *Actb-cre* mice (The Jackson Laboratory, stock L003376) to generate *Lats1*$^{D/+}$;*Lats2*$^{D/+}$ mice. These mice were then bred to *Shh*^{Cre} mice and the resulting progeny were bred to *Lats1*$^{flox/flox}$ and *Lats2*$^{flox/flox}$ to generate epithelial specific knockouts. *Spc-rtTA* mice were bred to teto-YAP^{S127A} mice, to *tetO-cre* and *Yap*$^{flox/flox}$;*Taz*$^{flox/flox}$ mice (The Jackson Laboratory, stock 027929) to generate constitutively active YAP mutant and YAP/TAZ conditional knockout mice, respectively.

Immunohistochemistry/immunofluorescent staining

Whole E10.5, E11.5 and E12.5 embryos and lungs of E17.5, E18.5 and postnatal day (P) 0 mice were fixed in 3.7% paraformaldehyde (Electron Microscopy Sciences) diluted in PBS. Samples were either stained as wholemounts using a DAB immunohistochemistry kit (Vector Laboratories) or embedded in paraffin or frozen in OCT (Electron Microscopy Sciences) for sectioning. Whole lungs and sections were immunostained using standard protocols (Branchfield et al., 2017). Primary antibodies used were: rabbit anti-phospho-YAP (1:500; Cell Signaling, 4911S), mouse anti-YAP (1:50; Santa Cruz Biotechnology, sc-101199), rabbit anti-YAP (1:200; Cell Signaling, 14074), rabbit anti-E-cadherin (1:200; Cell Signaling, 3195S), mouse anti-NKX2-1 (1:200; Thermo Fisher Scientific, MA5-13961), rabbit anti-aPKC (1:50; Santa Cruz Biotechnology, sc-208), goat anti-SCRIB (1:50; Santa Cruz Biotechnology, sc-11048), rabbit anti-LAMAα5 (1:200; kind gift of Dr Takako Sasaki, Oita University, Japan), rat anti-ITGB1 (1:200; Millipore, MAB1997), rabbit anti-HOPX (1:100; Santa Cruz Biotechnology, sc-30216), mouse anti-HOPX (1:50; Santa Cruz Biotechnology, sc-398703), Syrian hamster anti-PDPN (1:500; Developmental Studies Hybridoma Bank, 8.1.1.), rabbit anti-WNT5a (1:100; Abcam, ab174963) rabbit anti-pro-SPC (1:200; Seven Hills Bioreagents, WRAB-9337), rabbit anti-cleaved caspase 3 (1:100; Cell Signaling, 9661), rabbit anti-PH3 (1:500; Upstate Cell Signaling Solutions, 9701), mouse anti-SOX2 (1:50; Santa Cruz Biotechnology, sc-365823) rabbit anti-SOX9 (1:500; Millipore, AB5535). Slides were then incubated with FITC- or Cy3-conjugated secondary antibodies (1:200; Jackson ImmunoResearch: Cy3 goat anti-rabbit, 111-165-144; FITC goat anti-rabbit, 111-095-144; Cy3 goat anti-mouse, 115-165-003; FITC donkey anti-goat, 705-545-147; Cy3 goat anti-rat, 112-165-167; Cy3 goat anti-Syrian hamster, 107-165-142). Slides were mounted with Vectashield containing DAPI (Vector Laboratories) and visualized/photographed using a Zeiss AxioImager.A2 microscope and AxioCam MRc camera. Images were processed using Adobe Photoshop and/or ImageJ.

Immunostaining quantification

Three equally spaced, and equivalent slides from either controls or mutants were immunofluorescently stained for HOPX, pro-SPC or PH3. Three 20× (E11.5 PH3) or 40× (p0 PH3, HOPX, pro-SPC) images were taken from similar areas of each slide. For E11.5 PH3 quantification, the number of PH3$^+$ and DAPI$^+$ cells in the epithelium were counted to determine the percentage of proliferating epithelial cells. For P0 PH3, pro-SPC and HOPX quantification, the number immunopositive and DAPI$^+$ cells in the entire 40× field were counted to determine the percentage of positive cells. Statistical significance was determined using Student's *t*-test.

Quantitative RT-PCR (qRT-PCR)

RNA was isolated from embryonic and postnatal whole lungs using an RNEasy micro or mini kit (Qiagen), respectively, as per the manufacturer's protocol. RNA (0.5 µg) was reverse transcribed into cDNA using Superscript III (Invitrogen). A 'no RT' enzyme sample was also prepared and used as a negative control. For qRT-PCR, 0.1-0.33 µl of cDNA was amplified using gene-specific primers and SYBR Green mix (Bio-Rad) on a Bio-Rad MyiQ real-time PCR machine. Data were analyzed using the change in cycle threshold (ΔC_t) value method. Statistical significance was determined using Student's *t*-test. For a list of gene-specific primers, see Table S1.

Whole-mount *in situ* hybridization

Embryonic lungs were dissected in PBS, fixed in 4% paraformaldehyde overnight at 4°C, and then dehydrated to 100% methanol. Whole-mount *in situ* hybridization was carried out following established protocols (Abler et al., 2011).

Acknowledgements

We thank Drs Fernando D. Camargo and Eric Olson for sharing mouse lines, and members of the Sun laboratory for constructive discussions and readings of the manuscript.

Competing interests

The authors declare no competing or financial interests.

Author contributions

Conceptualization: L.B.N., X.S.; Methodology: L.B.N., R.L.J., X.S.; Validation: L.B.N., R.E.Y.; Formal analysis: L.B.N., R.E.Y., W.G.P., Y.Z., J.M.V.; Investigation: L.B.N., R.E.Y.; Resources: L.B.N., R.L.J., X.S.; Data curation: R.E.Y.; Writing - original draft: L.B.N., X.S.; Writing - review & editing: L.B.N., R.E.Y., W.G.P., J.M.V., X.S.; Visualization: L.B.N., R.E.Y., X.S.; Supervision: X.S.; Project administration: X.S.; Funding acquisition: R.L.J., X.S.

Funding

This work was supported by a National Institutes of Health postdoctoral training grant to the University of Wisconsin Genetics program (T32 GM007133); a National Heart, Lung and Blood Institute grant (F32 HL132483 to L.B.N.); a National Science Foundation Graduate Research Fellowship Program grant (DGE-1747503 to R.E.Y.); National Heart, Lung, and Blood Institute grants (RO1 HL142215, HL097134, HL122406); and a Wisconsin Partnership Program Grant funded by the School of Medicine and Public Health, University of Wisconsin-Madison (2897 to X.S.). Deposited in PMC for release after 12 months.

Supplementary information

Supplementary information available online at
http://dev.biologists.org/lookup/doi/10.1242/dev.163105.supplemental

References

Abler, L. L., Mehta, V., Keil, K. P., Joshi, P. S., Flucus, C. L., Hardin, H. A., Schmitz, C. T. and Vezina, C. M. (2011). A high throughput in situ hybridization method to characterize mRNA expression patterns in the fetal mouse lower urogenital tract. *J. Vis. Exp.* 2912.

Aragona, M., Panciera, T., Manfrin, A., Giulitti, S., Michielin, F., Elvassore, N., Dupont, S. and Piccolo, S. (2013). A mechanical checkpoint controls multicellular growth through YAP/TAZ regulation by actin-processing factors. *Cell* **154**, 1047-1059.

Boussadia, O., Kutsch, S., Hierholzer, A., Delmas, V. and Kemler, R. (2002). E-cadherin is a survival factor for the lactating mouse mammary gland. *Mech. Dev.* **115**, 53-62.

Camargo, F. D., Gokhale, S., Johnnidis, J. B., Fu, D., Bell, G. W., Jaenisch, R. and Brummelkamp, T. R. (2007). YAP1 increases organ size and expands undifferentiated progenitor cells. *Curr. Biol.* **17**, 2054-2060.

Chan, S. W., Lim, C. J., Guo, F., Tan, I., Leung, T. and Hong, W. (2013). Actin-binding and cell proliferation activities of angiomotin family members are regulated by Hippo pathway-mediated phosphorylation. *J. Biol. Chem.* **288**, 37296-37307.

Chang, C., Goel, H. L., Gao, H., Pursell, B., Shultz, L. D., Greiner, D. L., Ingerpuu, S., Patarroyo, M., Cao, S., Lim, E. et al. (2015). A laminin 511 matrix is regulated by TAZ and functions as the ligand for the α6Bβ1 integrin to sustain breast cancer stem cells. *Genes Dev.* **29**, 1-6.

Chen, J. and Krasnow, M. A. (2012). Integrin Beta 1 suppresses multilayering of a simple epithelium. *PloS One* **7**, e52886.

Chen, C.-L., Gajewski, K. M., Hamaratoglu, F., Bossuyt, W., Sansores-Garcia, L., Tao, C. and Halder, G. (2010). The apical-basal cell polarity determinant Crumbs regulates Hippo signaling in Drosophila. *Proc. Natl. Acad. Sci. USA* **107**, 15810-15815.

Chung, C., Kim, T., Kim, M., Song, H., Kim, T.-S., Seo, E., Lee, S.-H., Kim, H., Kim, S. K., Yoo, G. et al. (2013). Hippo-Foxa2 signaling pathway plays a role in

peripheral lung maturation and surfactant homeostasis. *Proc. Natl. Acad. Sci. USA* **110**, 7732-7737.
Desai, T. J., Brownfield, D. G. and Krasnow, M. A. (2014). Alveolar progenitor and stem cells in lung development, renewal and cancer. *Nature* **507**, 190-194.
Dong, J., Feldmann, G., Huang, J., Wu, S., Zhang, N., Comerford, S. A., Gayyed, M. F., Anders, R. A., Maitra, A. and Pan, D. (2007). Elucidation of a universal size-control mechanism in Drosophila and mammals. *Cell* **130**, 1120-1133.
Grzeschik, N. A., Parsons, L. M., Allott, M. L., Harvey, K. F. and Richardson, H. E. (2010). Lgl, aPKC, and Crumbs regulate the Salvador/Warts/Hippo pathway through two distinct mechanisms. *Curr. Biol.* **20**, 573-581.
Halder, G., Dupont, S. and Piccolo, S. (2012). Transduction of mechanical and cytoskeletal cues by YAP and TAZ. *Nat. Rev. Mol. Cell Biol.* **13**, 591-600.
Harfe, B. D., Scherz, P. J., Nissim, S., Tian, H., McMahon, A. P. and Tabin, C. J. (2004). Evidence for an expansion-based temporal Shh gradient in specifying vertebrate digit identities. *Cell* **118**, 517-528.
Harris, K. S., Zhang, Z., McManus, M. T., Harfe, B. D. and Sun, X. (2006). Dicer function is essential for lung epithelium morphogenesis. *Proc. Natl. Acad. Sci. USA* **103**, 2208-2213.
Heallen, T., Zhang, M., Wang, J., Bonilla-Claudio, M., Klysik, E., Johnson, R. L. and Martin, J. F. (2011). Hippo pathway inhibits Wnt signaling to restrain cardiomyocyte proliferation and heart size. *Science (New York, N.Y.)* **332**, 458-461.
Kim, N.-G., Koh, E., Chen, X. and Gumbiner, B. M. (2011). E-cadherin mediates contact inhibition of proliferation through Hippo signaling-pathway components. *Proc. Natl. Acad. Sci. USA* **108**, 11930-11935.
Lange, A. W., Sridharan, A., Xu, Y., Stripp, B. R., Perl, A. K. and Whitsett, J. A. (2015). Hippo/Yap signaling controls epithelial progenitor cell proliferation and differentiation in the embryonic and adult lung. *J. Mol. Cell Biol.* **7**, 35-47.
Lefevre, J., Short, K. M., Lamberton, T. O., Michos, O., Graf, D., Smyth, I. M. and Hamilton, N. A. (2017). Branching morphogenesis in the developing kidney is governed by rules that pattern the ureteric tree. *Development* **144**, 4377-4385.
Li, J., Wang, Z., Chu, Q., Jiang, K. and Tang, N. (2018). The strength of mechanical forces determines the differentiation of alveolar epithelial cells. *Dev. Cell* **44**, 297-312.e5.
Lin, C., Yao, E. and Chuang, P.-T. (2015). A conserved MST1/2-YAP axis mediates Hippo signaling during lung growth. *Dev. Biol.* **403**, 101-113.
Lin, C., Yao, E., Zhang, K., Jiang, X., Croll, S., Thompson-Peer, K. and Chuang, P. T. (2017). YAP is essential for mechanical force production and epithelial cell proliferation during lung branching morphogenesis. *Elife* **6**, e21130.
Liu, Z., Wu, H., Jiang, K., Wang, Y., Zhang, W., Chu, Q., Li, J., Huang, H., Cai, T., Ji, H. et al. (2016). MAPK-Mediated YAP Activation Controls Mechanical-Tension-Induced Pulmonary Alveolar Regeneration. *Cell Rep.* **16**, 1810-1819.
Mahoney, J. E., Mori, M., Szymaniak, A. D., Varelas, X. and Cardoso, W. V. (2014). The Hippo pathway effector yap controls patterning and differentiation of airway epithelial progenitors. *Dev. Cell* **30**, 137-150.
Metzger, R. J., Klein, O. D., Martin, G. R. and Krasnow, M. A. (2008). The branching programme of mouse lung development. *Nature* **453**, 745-750.
Mo, J. S., Park, H. W. and Guan, K. L. (2014). The Hippo signaling pathway in stem cell biology and cancer. *EMBO Rep.* **15**, 642-656.
Pan, D. (2010). The hippo signaling pathway in development and cancer. *Dev. Cell* **19**, 491-505.
Perl, A. K., Tichelaar, J. W. and Whitsett, J. A. (2002a). Conditional gene expression in the respiratory epithelium of the mouse. *Transgenic Res.* **11**, 21-29.
Perl, A.-K. T., Wert, S. E., Nagy, A., Lobe, C. G. and Whitsett, J. A. (2002b). Early restriction of peripheral and proximal cell lineages during formation of the lung. *Proc. Natl. Acad. Sci. USA* **99**, 10482-10487.
Piccolo, S., Dupont, S. and Cordenonsi, M. (2014). The biology of YAP/TAZ: Hippo signaling and beyond. *Physiol. Rev.* **94**, 1287-1312.
Reginensi, A., Enderle, L., Gregorieff, A., Johnson, R. L., Wrana, J. L. and McNeill, H. (2016). A critical role for NF2 and the Hippo pathway in branching morphogenesis. *Nat. Commun.* **7**, 12309.
Szymaniak, A. D., Mahoney, J. E., Cardoso, W. V. and Varelas, X. (2015). Crumbs3-mediated polarity directs airway epithelial cell fate through the hippo pathway effector Yap. *Dev. Cell* **34**, 283-296.
Szymaniak, A. D., Mi, R., McCarthy, S. E., Gower, A. C., Reynolds, T. L., Mingueneau, M., Kukuruzinska, M. and Varelas, X. (2017). The Hippo pathway effector YAP is an essential regulator of ductal progenitor patterning in the mouse submandibular gland. *Elife* **6**, e23499.
Volckaert, T., Yuan, T., Chao, C. M., Bell, H., Sitaula, A., Szimmtenings, L., El Agha, E., Chanda, D., Majka, S., Bellusci, S. et al. (2017). Fgf10-Hippo epithelial-mesenchymal crosstalk maintains and recruits lung basal stem cells. *Dev. Cell* **43**, 48-59.e5.
Walker, J. L., Menko, A. S., Khalil, S., Rebustini, I., Hoffman, M. P., Kreidberg, J. A. and Kukuruzinska, M. A. (2008). Diverse roles of E-cadherin in the morphogenesis of the submandibular gland: insights into the formation of acinar and ductal structures. *Dev. Dyn.* **237**, 3128-3141.
Xin, M., Kim, Y., Sutherland, L. B., Qi, X., McAnally, J., Schwartz, R. J., Richardson, J. A., Bassel-Duby, R. and Olson, E. N. (2011). Regulation of insulin-like growth factor signaling by Yap governs cardiomyocyte proliferation and embryonic heart size. *Sci. Signal.* **4**, ra70.
Xin, M., Kim, Y., Sutherland, L. B., Murakami, M., Qi, X., McAnally, J., Porrello, E. R., Mahmoud, A. I., Tan, W., Shelton, J. M. et al. (2013). Hippo pathway effector Yap promotes cardiac regeneration. *Proc. Natl. Acad. Sci. USA* **110**, 13839-13844.
Yates, L. L., Schnatwinkel, C., Hazelwood, L., Chessum, L., Paudyal, A., Hilton, H., Romero, M. R., Wilde, J., Bogani, D., Sanderson, J. et al. (2013). Scribble is required for normal epithelial cell-cell contacts and lumen morphogenesis in the mammalian lung. *Dev. Biol.* **373**, 267-280.
Zanconato, F., Forcato, M., Battilana, G., Azzolin, L., Quaranta, E., Bodega, B., Rosato, A., Bicciato, S., Cordenonsi, M. and Piccolo, S. (2015). Genome-wide association between YAP/TAZ/TEAD and AP-1 at enhancers drives oncogenic growth. *Nat. Cell Biol.* **17**, 1218-1227.
Zhao, B., Ye, X., Yu, J., Li, L., Li, W., Li, S., Lin, J. D., Wang, C. Y., Chinnaiyan, A. M., Lai, Z. C. et al. (2008). TEAD mediates YAP-dependent gene induction and growth control. *Genes Dev.* **22**, 1962-1971.
Zhao, R., Fallon, T. R., Saladi, S. V., Pardo-Saganta, A., Villoria, J., Mou, H., Vinarsky, V., Gonzalez-Celeiro, M., Nunna, N., Hariri, L. P. et al. (2014). Yap tunes airway epithelial size and architecture by regulating the identity, maintenance, and self-renewal of stem cells. *Dev. Cell* **30**, 151-165.

Figure S1

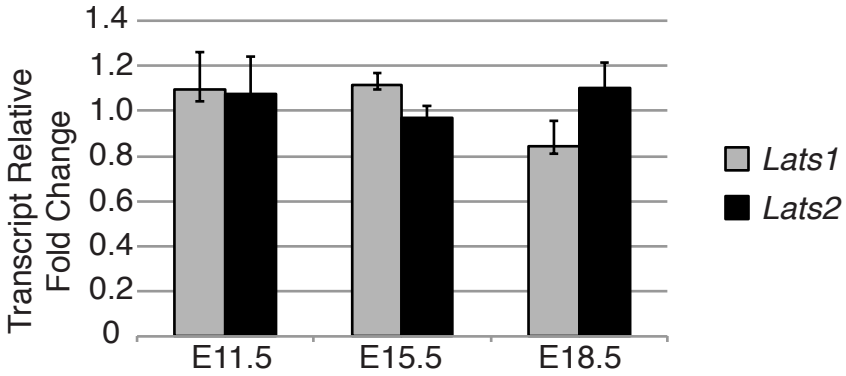

Figure S1. *Lats1* and *Lats2* relative mRNA levels remained unchanged throughout development.

(A) qRT-PCR quantification of mRNA levels of *Lats1* and *Lats2* relative to *β-Actin* (*Actb*) in control lungs at E11.5, E15.5 and E18.5. Data are presented as mean +/- SEM.

Figure S2

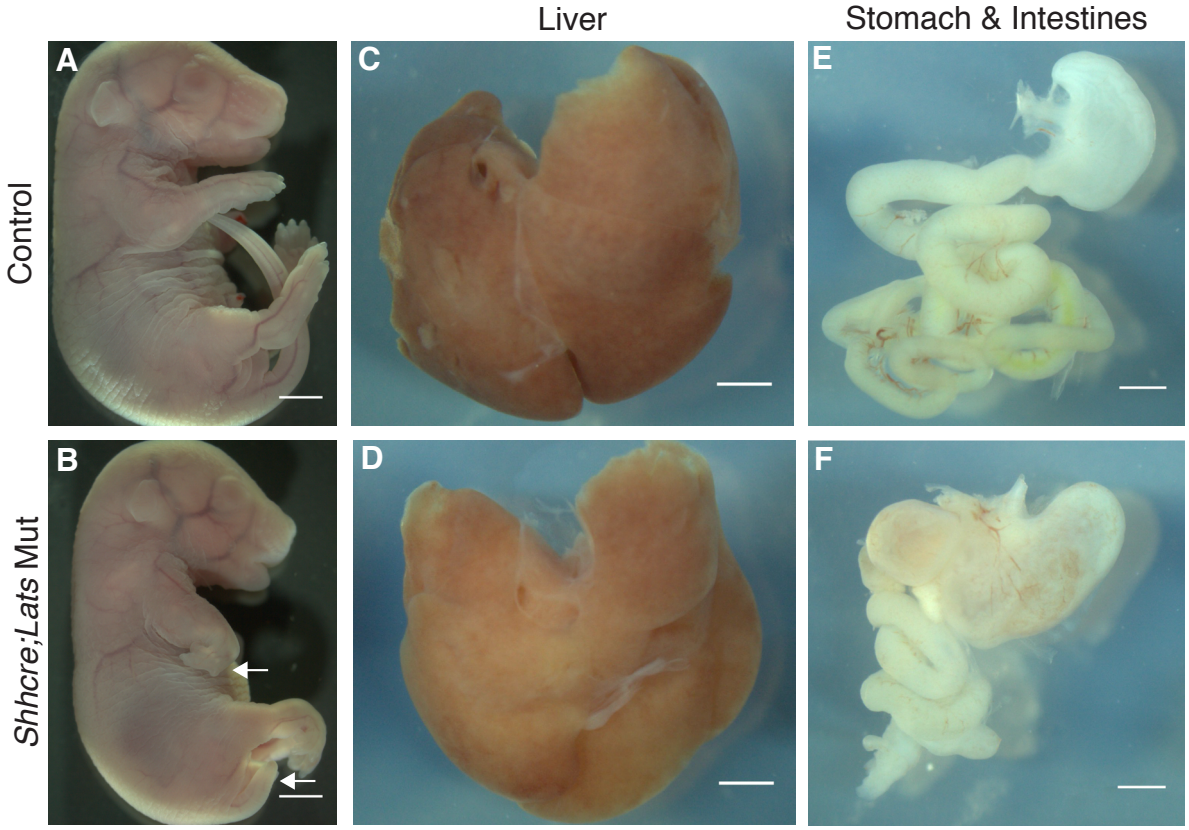

Figure S2. *Shhcre;Lats* mutants showed gross morphological defects. (A,B) Whole embryo images of control and the *Shhcre;Lats* mutant at E18.5 showed limb and tail defects (arrows). (C, D) Liver size in controls and *Shhcre;Lats* mutants appeared similar, likely due to low cre activity in the liver. (E,F) The stomach was larger but the intestine was shorter in the *Shhcre;Lats* mutants compred to the control. Scale bars: 50μm.

Figure S3

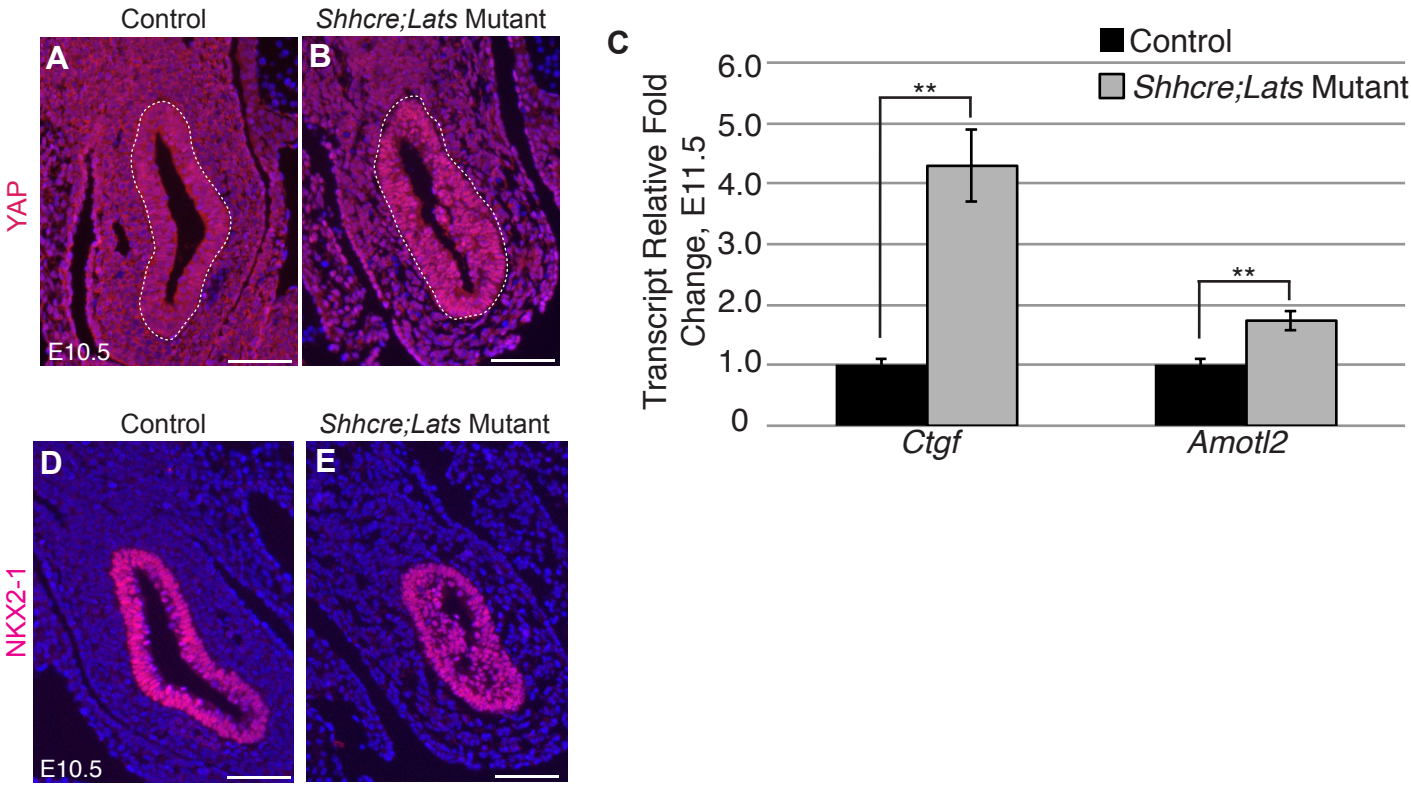

Figure S3. *Shhcre;Lats* mutants showed increased nuclear YAP at E10.5. (A,B) Immunofluorescent detection of YAP (red) in control and *Shhcre;Lats* mutant lungs at E10.5, showing intense nuclear staining in the mutant epithelium. (C) qRT-PCR quantification of relative mRNA levels of *Ctgf* and *Amotl2* in *Shhcre;Lats* mutant lungs at E11.5. **: $p<0.01$. Data are presented as mean +/- SEM. (D,E) Immunofluorescent detection of NKX2-1 (red) in control and *Shhcre;Lats* mutant lungs at E10.5, showing presence of signal in the mutant. Scale bars: 50μm.

Figure S4

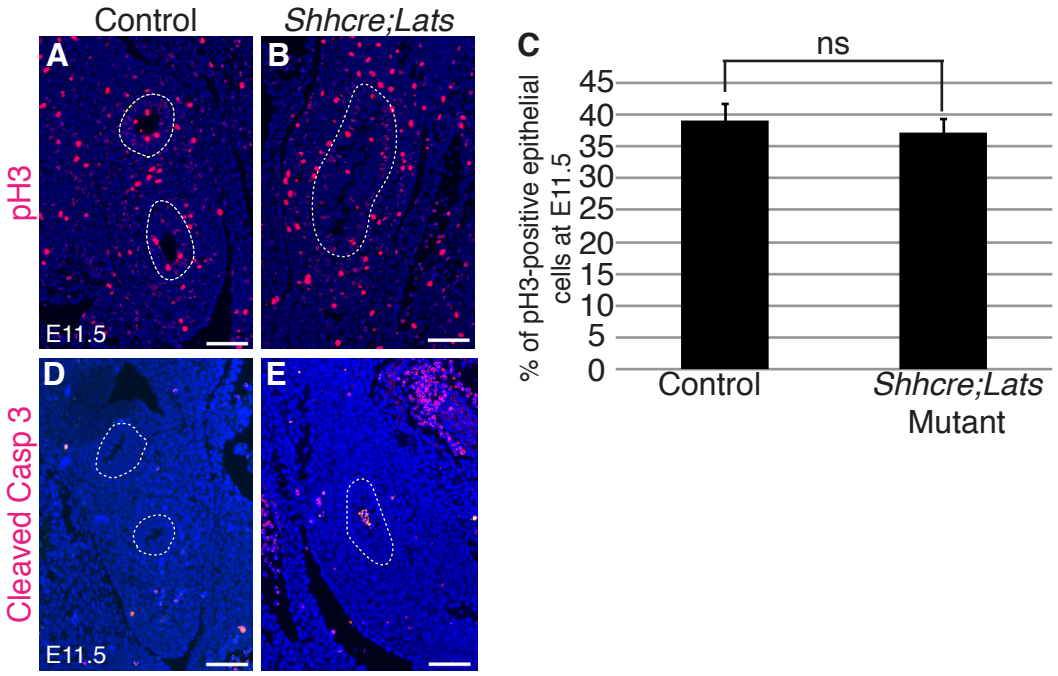

Figure S4. *Shhcre;Lats* mutants showed normal proliferation, but increased cell death at E11.5.

(A,B) Immunofluorescent detection of phospho-histone H3 (red) in control and *Shhcre;Lats* mutant lungs at E11.5, showing similar signals in the mutant as compared to control. Dotted circles outline the epithelium. (C) Quantification of percentage of epithelial cells positive for phospho-histone H3. ns: not significant. Data are presented as mean +/- SEM. (D,E) Immunofluorescent detection of cleaved caspase 3 (red) in control and *Shhcre;Lats* mutant lungs at E11.5, showing increased signal in the lumen of the mutant epithelium. Dotted line outlines the epithelium. Scale bars: 50μm.

Figure S5

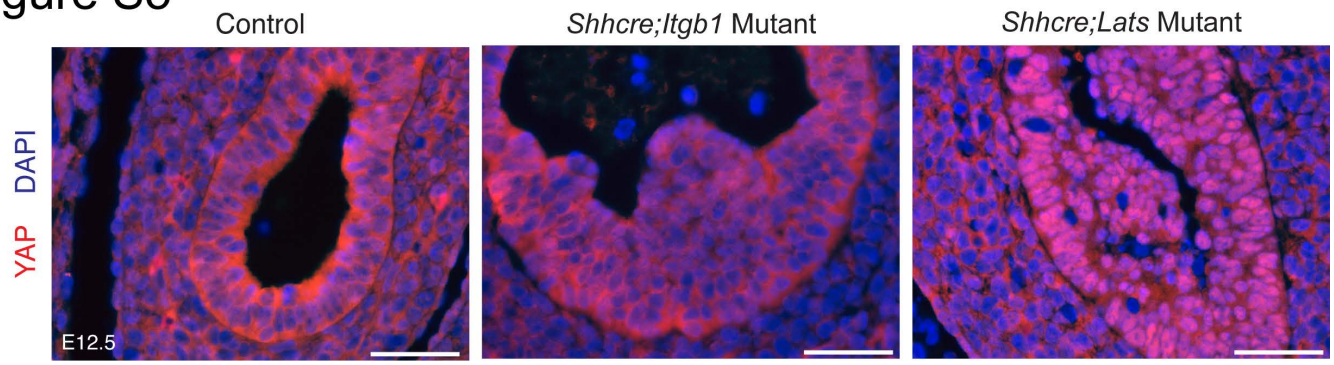

Figure S5. *Shhcre;Itgb1* mutants do not express YAP exclusively in the nucleus, unlike in *Shhcre;Lats* mutants.

(A-C) Immunofluorescent detection of YAP (red) and in E12.5 control, *Shhcre;Itgb1* and *Shhcre;Lats* lungs showing strong nuclear YAP expression in the epithelium of *Shhcre;Lats* mutants but not in *Shhcre;Itgb1* mutants. Scale bars: 50μm.

Figure S6

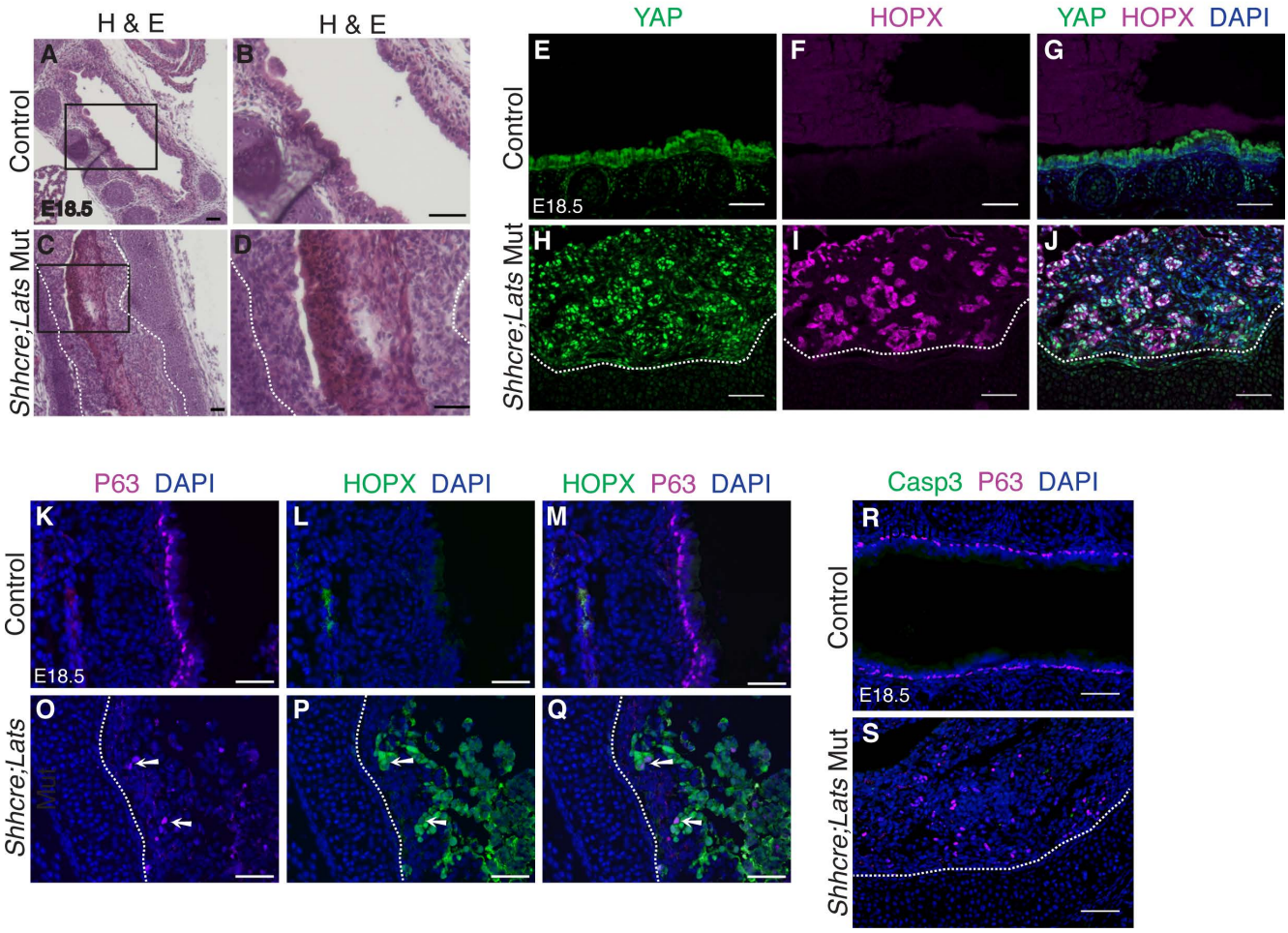

Figure S6. *Shhcre;Lats* mutants showed increased expression of AEC1 markers in the trachea at E18.5.

(A-B) Hematoxylin and Eosin staining of control and *Shhcre;Lats* mutant tracheas at E18.5. Boxed regions in A and C are magnified in B and D, which represent the general regions shown in the rest of the figure. In the mutant, the epithelium, delineated by white dashed lines, shows a large number of protruded cells that almost filled the lumen. (E-J) Immunofluorescent detection of YAP (green) and HOPX (magenta) in control and *Shhcre;Lats* mutant tracheas at E18.5, showing many YAP+ cells also express AEC1 marker HOPX in the *Shhcre;Lats* mutant tracheal epithelium, delineated by white dashed lines. (K-Q) Immunofluorescent detection of KRT5 (green) and P63 (magenta) in control and *Shhcre;Lats* mutant tracheas at E18.5, showing increased number and disorganization of KRT5+ and P63+ cells in the lumen of the mutant. White dashed lines delineate epithelium. (R,S) Immunofluorescent detection of cleaved Caspase 3 (green) and P63 (magenta) in control and *Shhcre;Lats* mutant tracheas at E18.5, showing presence and disorganization of P63+ cells, and few apoptotic cells in the mutant. White dashed lines delineate epithelium. Scale bars: 50μm.

Figure S7

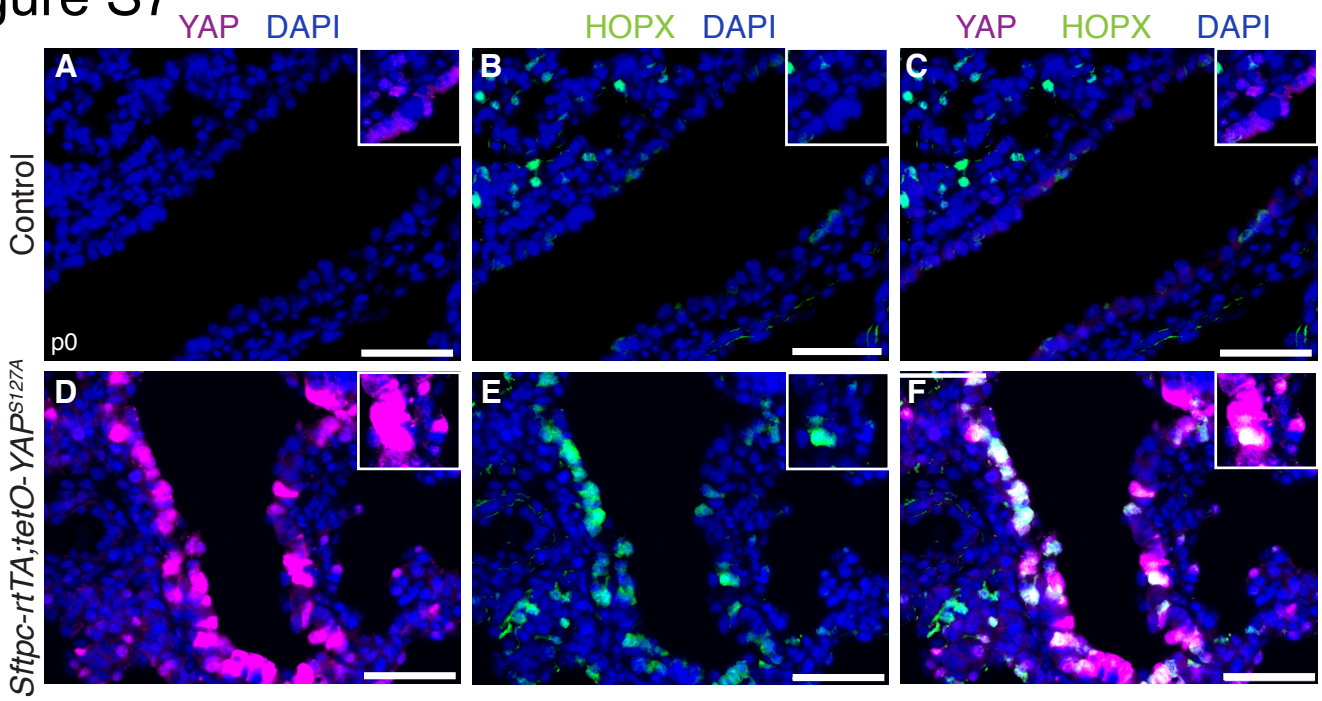

Figure S7. *Sftpc-rtTA;tetO-YAP*^{S127A} mutants showed ectopic HOPX expression in the airway epithelium.

(A-F) Immunofluorescent detection of HOPX (green) and YAP (magenta) in control and *Sftpc-rtTA;tetO-YAP*^{S127A} mutant lungs at p0, showing ectopic HOPX+ cells in the airway of trangenics. Insets show same staining adjusted for longer exposure to illustrate low YAP expression in control and high YAP expression in the mutant. Scale bars: 50μm.

Figure S8

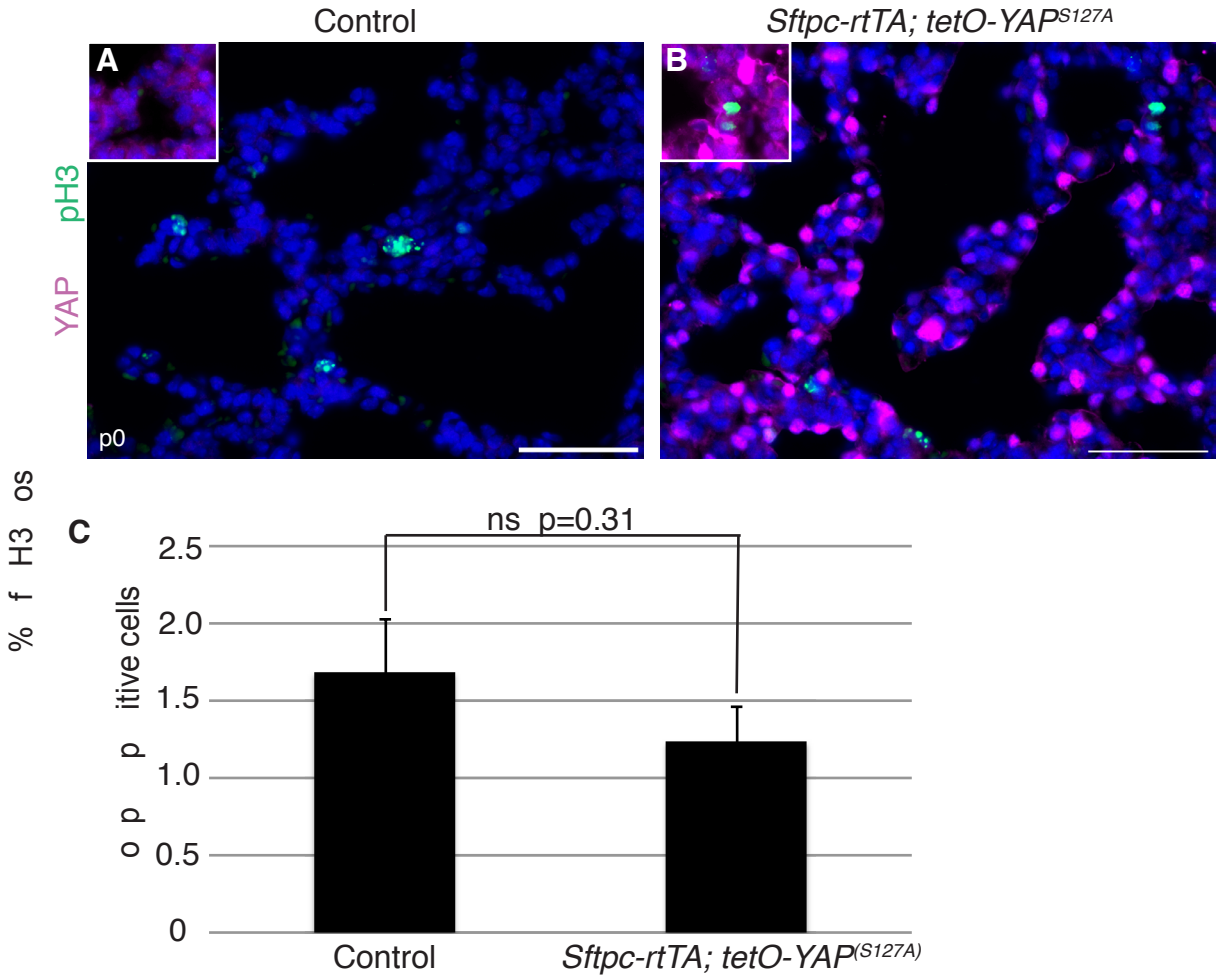

Figure S8. *Sftpc-rtTA;tetO-YAP*^{S127A} mutants did not show increased cell proliferation. (A,B) Immunofluorescent detection of phospho-Histone H3 (green) and YAP (magenta) in control and *Sftpc-rtTA;tetO-YAP*^{S127A} mutant lungs at p0. Insets show same staining adjusted for longer exposure to illustrate low YAP expression in control and high YAP expression in the mutant. Scale bars: 50μm. (C) Percentage of DAPI cells positive for phospho-Histone H3 (Control: 1.68 +/- 0.35% , Mutant: 1.25 +/- 0.23%, p=0.31). ns: not significant. Data are presented as mean +/- SEM.

Figure S9

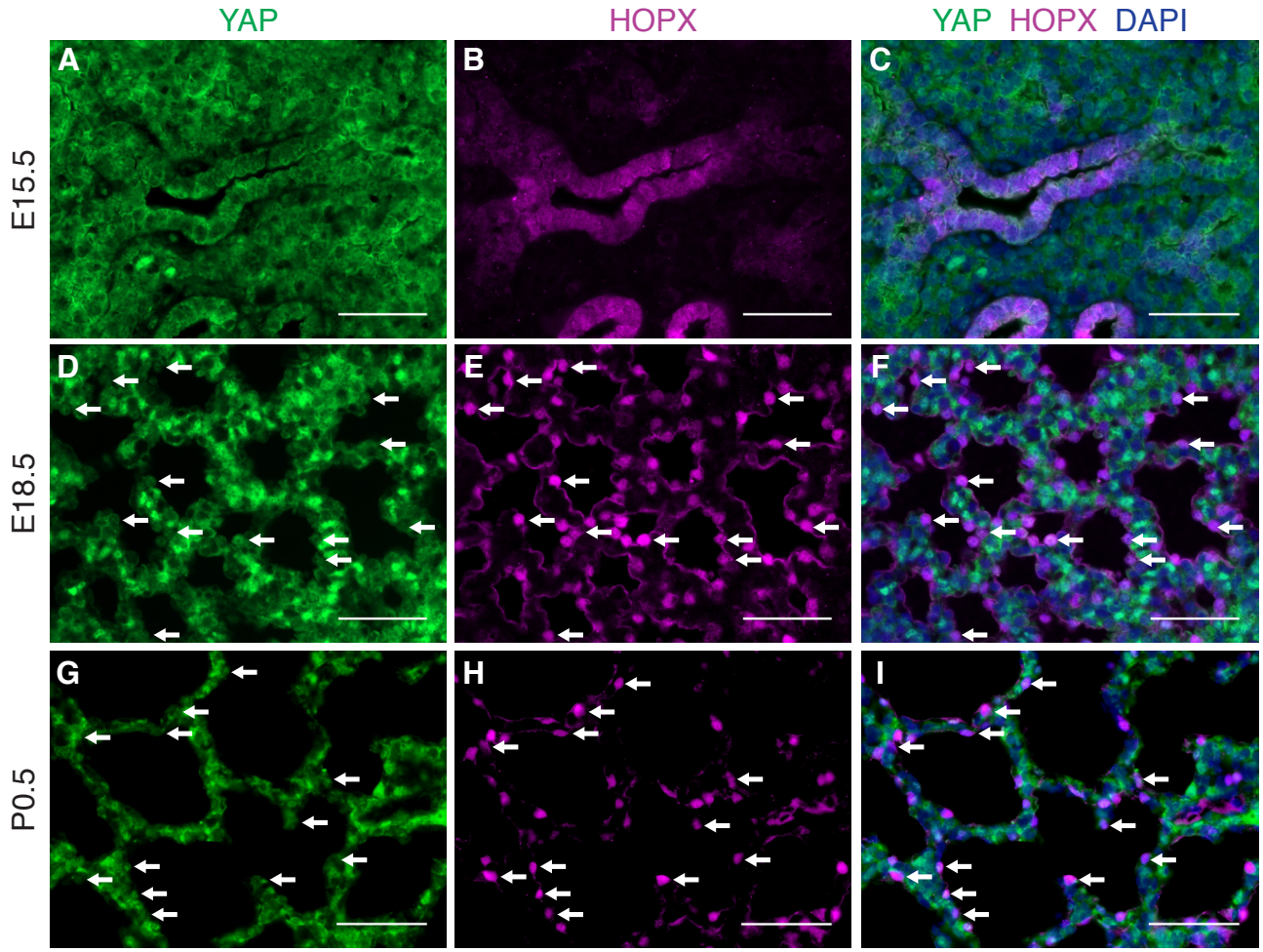

Figure S9. Nuclear YAP was detected in AEC1s in the normal lung.

(A-I) Immunofluorescent detection of YAP (green) and HOPX (magenta) in control lungs at E15.5, E18.5 and p0. At E18.5 and P0, but not E15.5, there are cells with nuclear YAP and HOPX expression (arrows). Scale bars: 50μm.

Figure S10

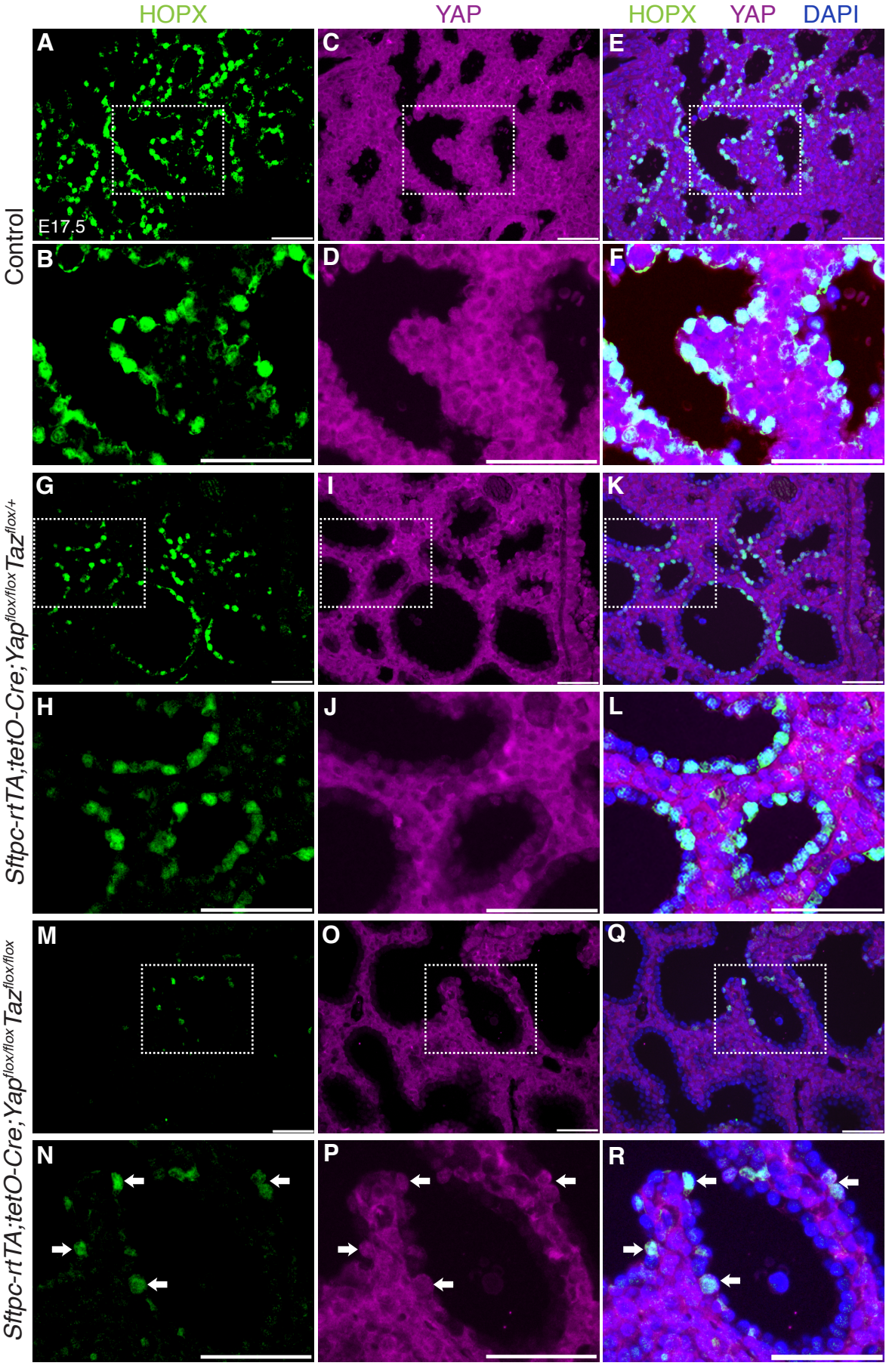

Figure S10. *Sftpc-rtTA;tetO-Cre;Yap$^{flox/flox}$;Taz$^{flox/flox}$* mutants showed that both *Yap* and *Taz* are essential for AEC1 differentiation.

(A-R) Immunofluorescent detection of HOPX (green) and YAP (magenta) in control, *Sftpc-rtTA;tetO-Cre;Yap$^{flox/flox}$;Taz$^{flox/+}$* mutant and *Sftpc-rtTA;tetO-Cre;Yap$^{flox/flox}$;Taz$^{flox/flox}$* mutant lungs at E17.5. Boxed areas are magnified in the rows immediately below. The *Sftpc-rtTA;tetO-Cre;Yap$^{flox/flox}$;Taz$^{flox/+}$* mutants showed an intermediate phenotype of slightly reduced HOPX+ cells. Arrows in the *Sftpc-rtTA;tetO-Cre;Yap$^{flox/flox}$;Taz$^{flox/flox}$* mutant indicated that the few remaining HOPX+ cells all had escaped recombination and retained YAP. Scale bars: 50μm.

Table S1. Primers used for qRT-PCR

Transcript	Forward Primer (5'-3')	Reverse Primer (5'-3')
Actb	CGGCCAGGTCATCACTATTGGCAAC	GCCACAGGATTCCATACCCAAGAAG
Ager	GTGGCTCAAATCCTCCCCAAT	CCTTCCCTCGCCTGTTAGTTG
Amotl2	AAGGGCTCGTATCCAGTGAG	CGTCTCTGCTGCCA TGTTT
Cdh1	CAAGGACAGCCTTCTTTTCG	TGGACTTCAGCGTCACTTTG
Ctgf	GCCCTAGCTGCCTACCGACT	AACAGGCGCTCCACTCTGTG
Hopx	CCACGCTGTGCCTCATCGCA	GGCCTGGCTCCCTAGTCCGT
Pdpn	CACCTCAGCAACCTCAGAC	AAGACGCCAACTATGATTCCAA
Sox2	GGAGAAAGAAGAGGAGAGAG	CTGGCGGAGAATAGTTGG
Sox9	CGTGGACATCGGTGAACTGA	GGTGGCAAGTATTGGTCAAACTC
Wnt5a	CAAATAGGCAGCCGAGAGAC	CTCTAGCGTCCACGAACTCC
Wnt7b	CAATGGTGGTCTGGTACCCAA	AGTCTCATGGTCCCTTTGTGGTT